

Abstract

WHITTINGTON, KURT THOMAS. A Tool to Extrapolate Thermal Reentry Atmosphere Parameters Along a Body in Trajectory Space. (Under the direction of Dr. Fred R. DeJarnette).

A critical component in designing a hypersonic vehicle is the ability to accurately predict the surface heating rates that determines the thermal protection system material that shields the structure and payload from the extreme heating that occurs while passing through the atmosphere. Navier-Stokes (N-S) based computational fluid dynamic (CFD) codes provide the best means to accurately simulate the aerothermodynamic environment of flight but they require a considerable amount of time and resources. N-S based CFD codes offer an invaluable tool during the detailed design stage where accuracy is most critical, but more efficient methods are needed when considering the hundreds of trajectories and geometries which are typical to analyze during the preliminary design stage.

This research aids in the current efforts to develop new methods to rapidly compute convective heating rates on hypersonic vehicles done by H. H. Hamilton III and K. J. Weilmuenster of the Aerothermodynamic Branch of NASA Langley Research Center and Dr. F. R. DeJarnette of North Carolina State University. As a follow-up to the work done by these individuals, the NASA branch has requested that the findings of these programs be correlated to predict heating rates along the entire trajectory of a planetary entry vehicle.

As presented in the report, a new approach has been developed which uses a combination of interpolation from a database of results previously computed and extrapolation by utilizing boundary layer and hypersonic based correlations. The results database can be constructed within a few days by using an approximation method to calculate a relatively small number of flowfield solutions about a vehicle. This approach

has been incorporated into a database tool called Extrapolate Thermal Reentry Atmosphere Parameters (xTRAP).

As tested with a spherical blunted-nose cone geometry, xTRAP is able to predict convective heating rates within seconds at any point throughout a defined trajectory space from a database of 26 previously calculated solutions. At angle-of-attacks from 25° to 45°, xTRAP has been shown to predict laminar and turbulent convective heating rates within 15% error along a body at freestream velocities of 10,000 to 20,000 ft/s. Therefore, xTRAP greatly reduces computational time and has proven to be a beneficial tool during the preliminary design of hypersonic vehicles.

© Copyright 2011 by Kurt Thomas Whittington

All Rights Reserved

A Tool to Extrapolate Thermal Reentry Atmosphere Parameters Along a Body
in Trajectory Space

by
Kurt Thomas Whittington

A thesis submitted to the Graduate Faculty of
North Carolina State University
in partial fulfillment of the
requirements for the degree of
Master of Science

Aerospace Engineering

Raleigh, North Carolina

2011

APPROVED BY:

Dr. William L. Roberts IV

Dr. Jack R. Edwards Jr.

Dr. Fred R. DeJarnette
Committee Chair

Dedication

Dedicated to my wife, Erin, for your love and support that encouraged me along the way and provided the means for me to pursue this goal and to my baby girl, Emma, whose birth gave me the motivation to finish.

Biography

Kurt Whittington was born into a Christian home in Brampton, Ontario, Canada on May 2, 1981. He developed an interest in aerospace studies from learning about the *Canadarm*, which is the robotic remote manipulator system used on the U.S. Space Shuttle and developed in his hometown. In July 1996, he accepted Christ's grace in baptism, and then in 1999 he moved to the United States to pursue an undergraduate degree in Mechanical Engineering at a Christian university.

During college, he managed the university's academic assistance program, worked as a mathematics and physics tutor and interned at Boeing Satellite Systems where his interest in aerospace discovery only grew. He met his wife working in the tutoring program and was very involved with a service ministry group called, *Outreach*, where he and his wife developed an interest in vocational ministry. He graduated, *Magna Cum Laude* from Oklahoma Christian University in 2003 with a degree in Mechanical Engineering with the intent to pursue Aerospace Engineering in graduate school. However, he felt compelled to first pay back school loans so he took a position as a Commissioning Engineer in the Pharmaceutical industry. Though he gained invaluable hands-on experience working in a validation test environment, his drive to understand and develop new solutions finally led him to pursue his dream in Aerospace Engineering.

Currently, Kurt is a master's student in Aerospace Engineering at North Carolina State University. Graduate school has narrowed his interests to aerothermal analysis in which he hopes to find employment as a research engineer upon graduation. Ultimately, he plans to return to academia to complete a Ph.D. and work as a Professor of Aerospace Engineering teaching young engineers the importance of scientific research.

Acknowledgments

I would like to extend my appreciation to my advisor and mentor, Dr. Fred DeJarnette, for introducing me to the field of aerothermodynamics that blended my experience in thermal-fluids and my interest in applied aerodynamics. Dr. DeJarnette served as the chairman of my advisory committee along with professors Dr. Jack Edwards and Dr. William Roberts to whom I also extend my thanks.

Also, I would like to acknowledge with sincere gratitude H. Harris Hamilton of the Aerothermodynamic branch at the Langley Research Center of the National Aeronautics and Space Administration (NASA) who tasked me on this effort and patiently supported me along the way. From going out of his way by accepting my phone calls while at home during the weekend and providing guidance that was invaluable to the success of this investigation, I extend my deepest appreciation.

Table of Contents

List of Tables	viii
List of Figures	ix
Nomenclature	x
Chapter 1 Introduction.....	1
1.1 Research Objectives	2
1.2 Extrapolation Program	3
Chapter 2 Background Theory.....	4
2.1 Reentry Trajectories	4
2.2 Reentry Temperatures	8
2.3 Aerodynamic Heating	8
Chapter 3 Aerothermodynamic Analysis	11
3.1 Experimental Measurements.....	11
3.2 Numerical Solutions	12
3.2.1 Navier-Stokes Code Solvers	13
3.2.2 Approximate Boundary Layer Solutions.....	14
3.2.3 Interpolation Programs	15
3.3 Analytical Solutions	15
3.3.1 Fay and Riddell	16
3.3.2 Generalized Heating Equations	16
Chapter 4 Requirements and Considerations.....	19
4.1 Requirements	19
4.1.1 Function	20
4.1.2 Efficiency	21
4.1.3 Accuracy	21
4.1.4 Ease of Use	22
4.2 Design Considerations	22
4.2.1 Trajectory and Geometry	23
4.2.2 Number of Data Points.....	23

	4.2.3 Interpolation	24
	4.2.4 Extrapolation.....	25
Chapter 5	Analysis and Design.....	27
	5.1 Analysis.....	27
	5.1.1 Extrapolation Procedure.....	27
	5.1.2 Known and Unknown Points	29
	5.1.3 Extrapolation Terms	31
	5.1.4 Stagnation Heating	34
	5.1.5 Extrapolation Factors.....	35
	5.2 Design.....	38
	5.2.1 Database and CFD Solutions.....	38
	5.2.2 Trajectory and Geometry	39
	5.2.3 Interpolation and Extrapolation.....	39
	5.2.4 Number of Data Points.....	40
	5.2.5 Operating xTRAP.....	41
	5.2.6 Resultant Data.....	41
Chapter 6	Validation and Results.....	43
	6.1 Validation	43
	6.1.1 Functional Testing.....	43
	6.1.2 Verification of Requirements.....	44
	6.2 Results	45
	6.2.1 Accuracy and Plots	46
	6.2.2 Observations and Discussion	51
Chapter 7	Conclusions and Recommendations.....	55
	7.1 Conclusions.....	55
	7.2 Recommendations.....	55
References	58
Appendices	61
	Appendix A - Cubic Spline Algorithm	62
	Appendix B - xTRAPs Main Screen (Screenshot)	65
	Appendix C - 25° Cone-Half Angle Plotted Results.....	67

Appendix D - 10° Cone-Half Angle Plotted Results.....	72
Appendix E - 45° Cone-Half Angle Plotted Results	75
Appendix F - Other Plotted Results	78

List of Tables

Table 4.1 - User Requirements.....	19
Table 6.1 - Functional Testing.....	43
Table 6.2 - Verification of Requirements.....	44
Table 6.3 - 25° Cone-half Angle Results	46
Table 6.4 - 10° Cone-half Angle Results.....	48
Table 6.5 - 45° Cone-half Angle Results	49
Table 6.6 - Other Results	50
Table 6.7 - xTRAP Operating Ranges	53

List of Figures

Figure 2.1 - Entry Corridor	5
Figure 2.3 - Deceleration and Heat Flux vs. Altitude	7
Figure 2.2 - Atmospheric Entry Trajectories on a Velocity-Altitude Map	7
Figure 2.4 - Heating Effects of Hypersonic Flow.....	10
Figure 5.1 - Baseline Trajectory with Deviation Limits.....	28
Figure 5.2 - Effects of Varying Cone-half Angle on Heating Rates Correlation	30
Figure 5.3 - Effects of Varying Altitude on Heating Rates Correlation	30
Figure 5.4 - Typical Velocity Correlation	33
Figure C.1 - 25° Results: Known Trajectory Points at $V_\infty = 16,000$ ft/s	68
Figure C.2 - 25° Results: Baseline Trajectory Points.....	69
Figure C.3 - 25° Results: 10% Above Baseline Trajectory Points.....	70
Figure C.4 - 25° Results: 10% Below Baseline Trajectory Points	71
Figure D.1 - 10° Results: Known Trajectory Points at $V_\infty = 16,000$ ft/s	73
Figure D.2 - 10° Results: 10% Above and Below Baseline Trajectory Points	74
Figure E.1 - 45° Results: Known Trajectory Points at $V_\infty = 16,000$ ft/s	76
Figure E.2 - 45° Results: 10% Above and Below Baseline Trajectory Points	77
Figure F.1 - Other Results: Midrange Points, 35° Cone-Half Angle.....	79
Figure F.2 - Other Results: Transition Point Examples ($x_t = 3.0$ ft)	79
Figure F.3 - Other Results: Random Scenarios	79
Figure F.4 - Other Results: Out-of-Range Scenarios, 25° Baseline	79

Nomenclature

A	constant dependent on angle-of-attack and geometry, <i>unknown</i>
Alt	altitude, <i>ft</i>
C_D	coefficient of drag, <i>dimensionless</i>
C_L	coefficient of lift, <i>dimensionless</i>
C_p	specific heat capacity under constant pressure, <i>ft-lb/(slugs-°R)</i>
CF_{ue}	correction factor for correlating velocity, <i>dimensionless</i>
g	gravitational acceleration, <i>ft/s²</i>
g_0	gravitational acceleration at sea-level, <i>ft/s²</i>
h	enthalpy, <i>ft-lb/slugs</i>
h_{aw}	adiabatic wall enthalpy, <i>ft-lb/slugs</i>
h_{cf}	heat transfer rate coefficient, <i>slugs/(ft²-s)</i>
h_D	diffusion enthalpy, <i>ft-lb/slugs</i>
L	length of the body, <i>ft</i>
Le	Lewis number, <i>dimensionless</i>
m	mass, <i>slugs</i>
p	pressure, <i>lb/ft²</i>
Pr	Prandtl number, <i>dimensionless</i>
q	heat flux per unit area, <i>BTU/(ft²-s)</i>
q_c	convective heat flux per unit area from gas to wall, <i>BTU/(ft²-s)</i>
q_R	radiative heat flux per unit area from gas to wall, <i>BTU/(ft²-s)</i>
q_{RS}	radiative heat flux per unit area from surface to gas, <i>BTU/(ft²-s)</i>
R	gas constant, <i>ft-lb/(slugs-°R)</i>
R_c	radius of curvature, <i>ft</i>
R_N	nose radius, <i>ft</i>
r	recovery factor, <i>dimensionless</i>
S	reference area, <i>ft²</i>
s	distance along the surface of the body, <i>ft</i>
T	temperature, <i>°R</i>

u	velocity in the x-direction, <i>ft/s</i>
V	total velocity, <i>ft/s</i>
V_E	entry velocity, <i>ft/s</i>
x	distance from leading edge, <i>ft</i>
x_T	distance from transition point, <i>ft</i>
α	angle-of-attack, <i>degrees</i>
θ	entry angle, <i>degrees</i>
μ	viscosity, <i>lb-s/ft²</i>
ξ	running length from start of the streamline, <i>ft</i>
ρ	density, <i>slugs/ft³</i>
X	Extrapolation factor, <i>dimensionless</i>

Subscripts

e	at the edge of the boundary layer
L	laminar flow
s	at the stagnation point
T	turbulent flow
w	at the wall
0	total
1	known point in trajectory space
2	unknown point in trajectory space
∞	freestream condition

Chapter 1

Introduction

The ability to accurately predict surface heating rates has proven to be one of the most significant issues to the design and development of planetary entry vehicles. This element as well as the shear and pressure forces used to calculate the aerodynamic behavior are fundamental to the analysis and design of the thermal protection system (TPS). The role of the TPS is to function as an effective insulator to protect the structure and payload of the spacecraft by ensuring, so called, *burn-through* of the outer wall of the vehicle does not occur due to the searing heat encountered during atmospheric entry. Proper TPS design is vital to prevent a possible disaster to planetary entry vehicles and crew. A common cited example is the disaster of Space Shuttle Columbia which occurred on February 1, 2003 when the orbital disintegrated during atmospheric entry due to hot-gases penetrating the wing structure resulting in the death of all seven crew members. Though the design of the TPS was not deemed at fault because the final accident investigation report determined that the TPS panel on the leading edge of the left wing was damaged from debris during launch¹, it is an example of the grave consequences that can exist without proper TPS insulation.

Due to experimental facilities inability to simultaneously simulate the various areas that make up the aerothermodynamic environment of flight (forces and moments, pressure distributions and the heating distribution), it is necessary to rely on computational fluid dynamics (CFD) codes to calculate these flowfields². Primarily these flowfields and heating rates are calculated using detailed and time consuming Navier-Stokes (N-S) based code solvers. Although they deliver the most accurate solutions, these complex N-S solvers require a considerable amount of run-time so it is not cost effective to rely

solely on full N-S solutions when considering the hundreds of trajectories and geometries which are typical during the conceptual stage of the vehicle design process. Although Navier-Stokes solvers serve a significant role in detailed design analysis, the current focus is to develop accurate and more efficient approximate engineering codes to be used during preliminary or conceptual design. With an accurate definition of the aerothermodynamic environment, better estimates can be made of TPS weight and other properties earlier in the design process, which will improve the overall vehicle development.

1.1 Research Objectives

This research is to aid in the current efforts to develop new methods to rapidly compute convective heating rates on hypersonic vehicles done by H. H. Hamilton III and K. J. Weilmuenster of the Aerothermodynamic Branch of NASA Langley Research Center and Dr. F. R. DeJarnette of North Carolina State University. Previous work has largely been focused on developing more efficient inviscid and boundary layer approximate codes that when used in conjunction compare favorably with N-S calculations.

As a follow-up to the work done by these individuals, the NASA branch has requested that the findings of these programs be correlated to predict heating rates along the entire trajectory of a planetary entry vehicle. Although accurate boundary layer code solvers, such as UNLATCH,^{3,4} have now been developed to rapidly compute heating rates at a single trajectory point, it is still considered too time consuming to compute the large number of solutions required throughout the trajectory space when designing a hypersonic vehicle. Therefore, the logical next progression to reduce the time to obtain the solutions is to construct the solutions using interpolation from a database of results previously computed. In this approach, known solutions are populated in a database for a particular vehicle shape and then the database is used to interpolate results that approximate the CFD solutions at various other points in the defined trajectory space. This allows heating results to be predicted very quickly based on data calculated previously without the need to run a full CFD solution at every trajectory point. Similar approaches have been developed in the past,^{5,6} however, when relying strictly on

interpolation it still requires a relative large number of database solutions. Since every time the vehicle configuration changes a new database is required to be generated, a much faster method to construct the approximate solutions is needed for preliminary design where the vehicle shape may undergo numerous changes.

1.2 Extrapolation Program

As presented in the report, a new approach to this problem has been developed which uses a combination of interpolation and extrapolation by utilizing boundary layer and hypersonic based correlations. When this new approach is combined with the use of an approximation method of solving the flowfield about a vehicle, such as with UNLATCH^{3,4}, then the database needed to construct the solutions can be populated within a few days using a relatively small number of known solutions in the database. Once the database is populated, this approach will give results within seconds of the heating rates at specified points along the body of a given vehicle based on the inputted flight conditions. Thus, the rapid nature of its solution allows quick adjustments to be made to the flight conditions, to predict heating rates at various other locations throughout the defined trajectory space. This method has been incorporated into a database tool called Extrapolate Thermal Reentry Atmosphere Parameters (xTRAP) which is the main development of this research.

Chapter 2

Background Theory

There are four critical parameters to consider when designing a vehicle for planetary entry - maximum heating rate, total heat load, maximum deceleration and maximum dynamic pressure. The maximum heating rate and maximum dynamic pressure determine the type of TPS material while the total heat load influences the thickness of the insulating material. Maximum deceleration becomes a major factor for manned flight missions because human beings are limited by the amount of deceleration they can withstand over a certain amount of time.

2.1 Reentry Trajectories

For manned reentry, it is important to safely define the *overshoot boundary* and *undershoot boundary* of allowable trajectories that make up the entry corridor into which the vehicle must be guided for a successful return to the surface. If the entry angle is too shallow, the vehicle will not sufficiently penetrate the atmosphere to have enough drag to be captured by the planet's gravitational pull but instead will skip-through the atmosphere back into outer space. On the other hand, if the entry angle is too steep the vehicle will penetrate the atmosphere too quickly and the amount of deceleration will be too great for humans aboard to safely withstand (Fig. 2.1)⁷. The trajectory along the overshoot boundary will have the highest total heat load which influences the TPS thickness while the trajectory along the undershoot boundary has the maximum heating rate and dynamic pressure which will be the basis for selecting the TPS material.

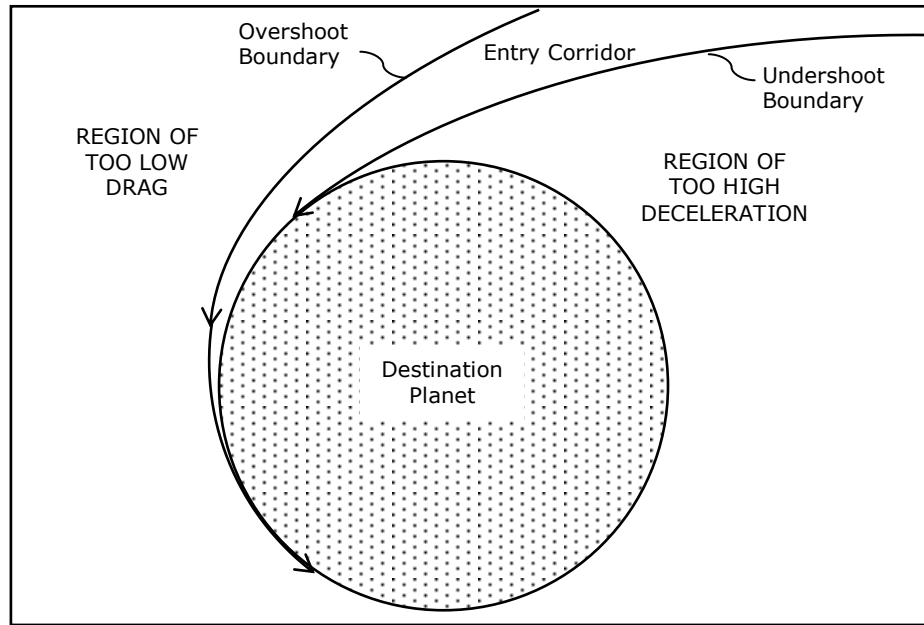


Figure 2.1 - Entry Corridor

A vehicle in Low-Earth-Orbit (LEO), such as the Space Shuttle docked at the International Space Station, will enter the Earth's atmosphere upon its return at speeds of approximately 7.9 km/s (25,919 ft/s, greater than Mach 25) – known as *orbital* or *satellite velocity*. While bodies entering Earth's atmosphere from a lunar mission, such as one of the Apollo capsules, or an interplanetary mission, such as a possible return from Mars, will have entry speeds of 11.2 km/s (36,745 ft/s, greater than Mach 35) or more – known as *escape velocity*⁷. The Space Shuttle's body and large angle-of-attack provide lift so it performs what is called a *lifting* or *glide entry*. However, the Apollo capsules had negligible lift so they performed what is called a *ballistic entry* and essentially fall through the atmosphere under the influence of only drag and gravity (Fig. 2.2)⁷. In both cases, it is advantageous to use a blunt body vehicle to increase pressure drag and naturally slow down the vehicle's velocity. However, as an even more important benefit, the use of a blunt-nose body in flight above sonic velocity causes a detached bow shock wave to be formed ahead of the vehicle. This bow shock minimizes skin friction drag and thus deflects some of the hot gases from being in direct contact with the vehicle, resulting in reduced surface heating rates.

As derived in various astronomical textbooks, the relationship relating freestream velocity to density in a lifting and ballistic entry is shown below in Equations 2.1 and 2.2, respectively⁷.

$$V^2 = \frac{g}{\frac{\rho}{2} \left(\frac{m}{C_L S} \right)^{-1} + \frac{1}{R_c}} \quad (2.1)$$

$$\frac{V}{V_E} = \exp \left(\frac{-\rho}{2 \left(\frac{m}{C_D S} \right) \left(\frac{g_0}{RT} \right) \sin(\theta)} \right) \quad (2.2)$$

Equation 2.1 is largely dependent on $m/(C_L S)$, called the *lift parameter*, which is related to the geometry of the entry vehicle. The R_c in Equation 2.1 represents the radius of curvature, which, in the case of entry to Earth's atmosphere, it is applicable to use the average radius of Earth (approx. 6.4e6 m or 2.09e7 ft)⁷. Likewise, Equation 2.2 is largely dependent on $m/(C_D S)$, which is also a product of the geometry of the vehicle but called the *ballistic parameter*. (Note: Equation 2.2 assumes an exponential model of the atmosphere to relate density to altitude.)

Figure 2.2 was created using Equations 2.1 and 2.2 with the lift and ballistic parameters listed in the legend. As shown, while penetrating the atmosphere at high altitudes the dominate effect of increasing density causes the deceleration to increase, but at lower altitudes the decrease in velocity dominates so the vehicle will reach a maximum deceleration at a specific altitude. Likewise, the heating rate will reach a maximum at a specific altitude. This altitude will always be higher than the altitude of maximum deceleration because heat flux is proportional to V_∞^3 while deceleration is proportional to V_∞^2 . As alluded to earlier, the maximum deceleration and maximum heating rates are two critical values to determine when making design considerations (Fig. 2.3).

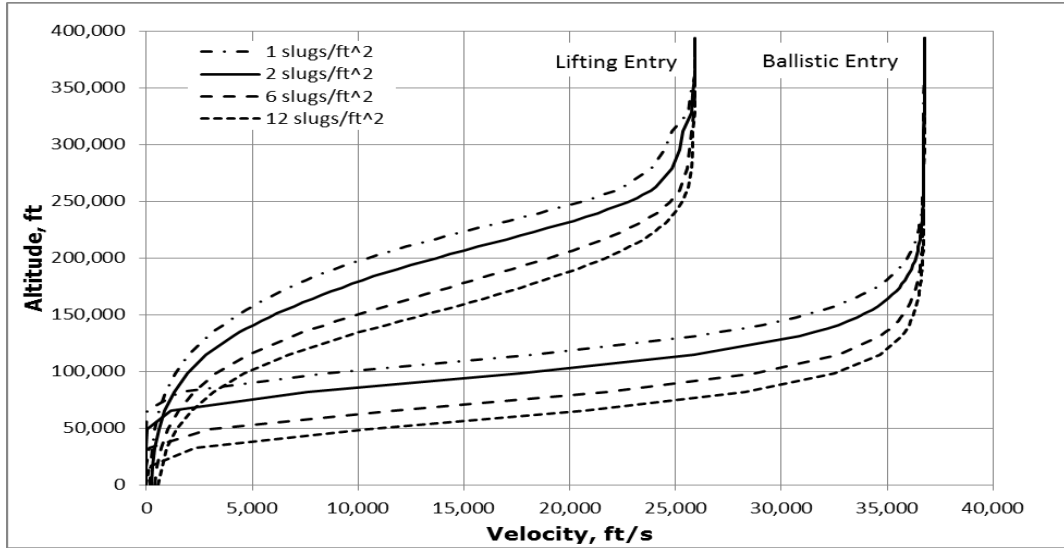


Figure 2.2 - Atmospheric Entry Trajectories on a Velocity-Altitude Map

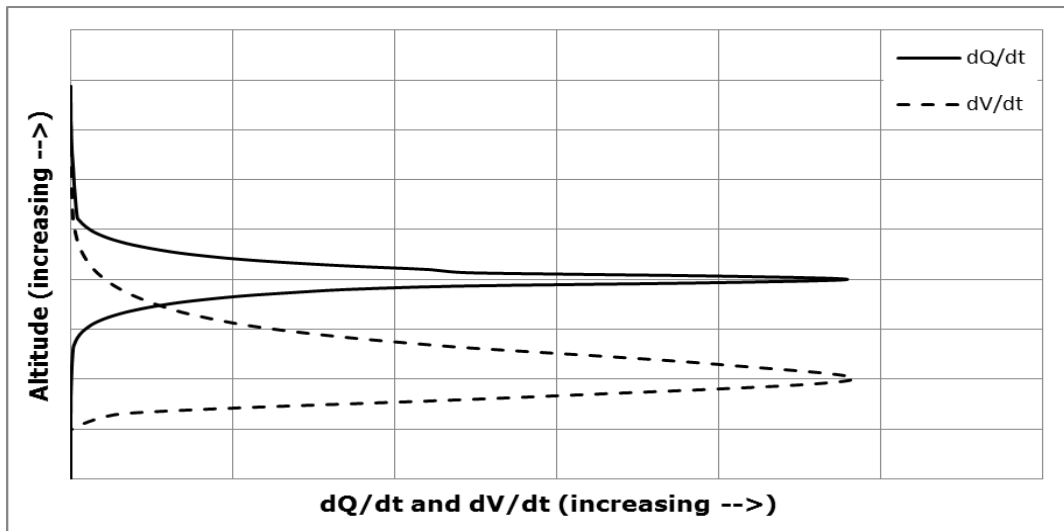


Figure 2.3 - Deceleration and Heat Flux vs. Altitude

2.2 Reentry Temperatures

A vehicle moving at hypersonic flight speeds will have a strong shock formed ahead of the body which converts most of the kinetic energy associated with the flight velocity into thermal and chemical energy⁸. Such is the case during direct planetary entry as seen in the example of the Apollo capsule when the temperatures in the shock layer in the nose region of the vehicle reached 11,000 K during its return through Earth's atmosphere⁹.

These extreme temperatures cause the atmospheric gases to no longer function as perfect gases with constant specific heats. The air that makes up the Earth's atmosphere is primarily a binary mixture of nitrogen and oxygen¹⁰, but at typical reentry velocities and temperatures the air compressed in the shock layer becomes both dissociated and ionized. With increasing temperatures, higher energy modes are excited - molecules vibrate called *vibrational excitation*, break apart called *dissociation* and then *ionization* occurs which is when electrons are released from the atoms leaving positive and negative charged ions. All of these *real gas* effects cause the air to stray from typically assumed perfect gas behavior and must be accounted for when analyzing the aerodynamic heating of a vehicle.

Since a reentry vehicle enters the atmosphere with such large kinetic and potential energy, which is primarily converted to heat during the descent, the priority during design is to deflect as much thermal energy as possible away from the vehicle in order to minimize the thermal energy that goes into the body.

2.3 Aerodynamic Heating

In the majority of cases during planetary entry, heat is transferred from the surrounding gas into the body, which is called *aerodynamic heating*. Aerodynamic heating occurs in the form of thermal radiation and thermal convection. Thermal radiation heating is caused from the incandescent shock layer gases¹¹ that become present from dissociation and ionization at high temperatures while convection heating is related to the hot gas in

the flowfield around the body. Thermal radiation is not a significant source of aerodynamic heating until the gas temperatures are high enough that the fluid elements radiate a substantial amount of energy. This threshold temperature for air is about 10,000 K⁹ which, as noted in Section 2.2, was reached in the shock layer in the nose region of the Apollo capsule during its reentry to Earth. In this case, the thermal radiation accounted for more than 30% of the total aerodynamic heating to the body surface⁹ but, in the possible case of atmospheric entry to Jupiter, the thermal radiation would account for more than 95% of the total heating. Since, this report focuses on atmospheric entry to Earth from LEO such as from the International Space Station, the effects of thermal radiation heating is beyond the scope of this document.

Convective heating that occurs in the boundary-layer adjacent to the body as the vehicle passes through the surrounding atmosphere is due to frictional forces because the kinetic energy of the flow velocity is dissipated into internal energy, called *viscous dissipation*. However, this heating is compounded by what is known as *shock-wave heating* which occurs from the hot compressed gas ahead of the vehicle and behind the very strong shock that forms as a result from the extreme velocities reached during reentry⁹. Also, as a point of interest, as the wall temperature increases, there will be thermal radiation from the wall surface as some of the heat will radiate away from the vehicle (Fig. 2.4¹⁰).

Therefore the heating rate at the wall, q_w , can be calculated by the following equation:

$$q_w = q_c + q_R - q_{RS} \quad (2.3)$$

However, for the purpose of this research with radiative heat transfer to and from the wall neglected, the convective heat transfer q_c will be denoted by q_w .

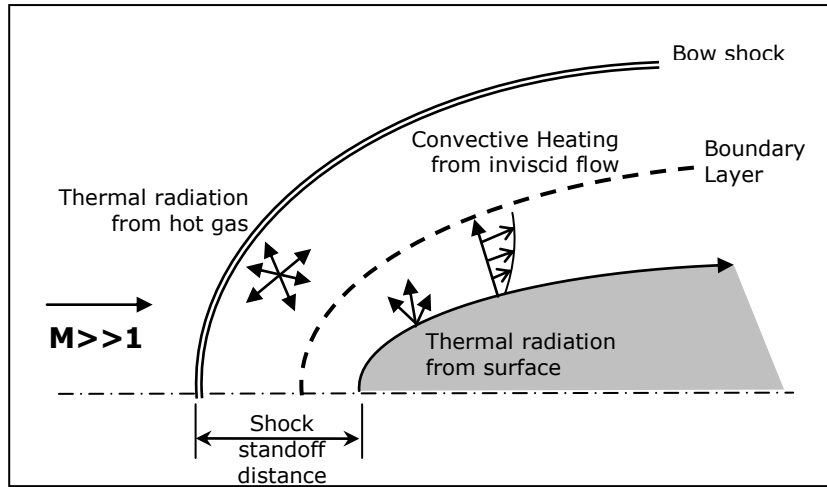


Figure 2.4 - Heating Effects of Hypersonic Flow

Chapter 3

Aerothermodynamic Analysis

The hypersonic vehicle design process integrates experimental, numerical and analytical testing techniques along with flight tests data to analyze aerodynamic heating and properly define the aerothermodynamic environment present during a vehicle's flight mission. Only full-scale flight tests provide an actual representation of a vehicle's environment but, of course, this testing method is too expensive and impractical because it can only occur once extensive design has been completed². Due to rising costs and the inability of other methods to predict the aerothermodynamic environment, there is an increasing reliance on numerical, or rather, computational testing methods but this reliance does not diminish the importance of incorporating other testing methods. The following serves as a literary search sampling some of the various aerothermal analysis methods commonly used today.

3.1 Experimental Measurements

Experimental testing involves measuring data in a ground-based facility such as a wind tunnel, shock tube, arc-heated tunnel, ballistic range enclosure or on a sled rail test platform. Since no one facility can simultaneously simulate the higher Mach numbers and high flowfield temperatures of the hypersonic flight environment¹², various facilities are used to test different aspects of hypersonic flight. For instance, to simulate altitude in a wind tunnel, a freestream static pressure is chosen that corresponds to the pressure at a given altitude for standard atmosphere⁹. However, the freestream static temperature is rarely adjusted to the corresponding standard atmosphere temperature,

but, as in some cases, it is lowered to decrease the speed-of-sound and simulate an increase in the freestream Mach number. Although, these methods are effective to achieve their desired specific result, they do not simultaneously simulate the environment of flight. However, when used in collaboration, ground-based testing can adequately obtain aerodynamic forces and moments, pressure distributions and predict the heat transfer distributions.

Compared to computational testing, the time required to fabricating models and conducting various test procedures can make experimental testing time and cost inefficient. However, experimental testing still serves a vital role in modern aerothermodynamics because experimental testing is used complementary to computational testing to provide data to develop realistic computational flow models and then validate, calibrate and compare results obtained from developed computer codes.

3.2 Numerical Solutions

Numerical experiments are used to effectively calculate heat flux distributions by using computational methods which consist of computational fluid dynamic (CFD) codes and/or approximate engineering codes. In order of least-to-greatest accuracy and complexity, CFD codes range from the *Viscous-Shock-Layer (VSL)*, to *Parabolized Navier-Stokes (PNS)* to *Full Navier-Stokes* methods⁹. Engineering codes however, are mainly boundary-layer approximations so they have a lower-fidelity but are computationally more efficient than CFD solutions. In general, computational codes solve a discretized form of the conservation laws that govern fluid flow such as the conservation of mass, momentum and energy. Time spent developing computational solutions consists of generating grids to sub-divide the vehicle's surface and surrounding sub-space into a finite number of elements and developing the algorithms that when executed will simulate the interaction of the fluid with the vehicle's surface boundaries.

The benefits of computational codes are that they provide detailed solutions, are relatively inexpensive to develop and are easy to modify for different flight conditions. Also, computational simulations provide the best means, next to actual flight testing, to fully capture all aspects of the aerothermodynamic environment. The disadvantages of

many detailed computational codes are the complex geometries and long run-times required to execute the solutions.

Various computer codes have been developed to calculate radiative and convective heating rates. However, due to the focus of this report, only some of the convective heating codes are summarized below.

3.2.1 Navier-Stokes Code Solvers

Full Navier-Stokes (N-S) code solvers provide the most accurate detailed solutions of surface heating rates of hypersonic reentry vehicles as validated based on measured flight data. Therefore, their ability to accurately predict aerothermal loading has proved to be an invaluable resource to the design of thermal protection systems.

One such N-S solver is the Langley Aerothermodynamic Upwind Relaxation Algorithm (LAURA) which has been used as a benchmark to validate various other code solvers and experimental testing methods. LAURA is a structured, multi-block, computational aerothermodynamic simulation code that uses a finite-volume approach to solve the inviscid, thin-layer Navier-Stokes, or full Navier-Stokes flowfield equations¹³.

Detailed N-S solvers require considerable computer storage requirements and long run-times so they are often a too expensive form of testing. For a typical reentry vehicle configuration most N-S solvers compute tens-of-million calculations to obtain a solution. As expected, this magnitude of calculations requires a large cluster of processing workstations and still results in run-times typical of 1-3 weeks to obtain a single solution. Time and resources cost money, so full N-S solvers should only be used when accuracy is most critical.

As summarized below, you'll see that approximate boundary layer (BL) codes have been developed to alleviate this problem. However, it is important to note that, N-S codes also have the ability to solve many flow conditions that BL codes cannot handle such as flow separation and other consequences of shock-wave/boundary layer interactions⁹.

3.2.2 Approximate Boundary Layer Solutions

Effective BL code solvers implement applicable hypersonic approximations to the equations that govern fluid flow to reduce their computation time while minimizing the loss in accuracy. These viscous codes use boundary layer theory formulas which first require the inviscid solution to be computed to determine the boundary layer edge conditions required to complete the viscous calculations. Various BL codes have been developed to function in conjunction with the various developed inviscid flow solvers.

SABLE:

SABLE is a finite-difference code for laminar or turbulent boundary layer solutions over axisymmetric bodies developed in 1992¹⁴. It can compute solutions using ideal gas, carbon tetrafluoride (CF₄) or equilibrium air chemistry. SABLE computes boundary layer solutions within seconds that compare favorably with N-S solutions, but its limitation is that it must work in conjunction with a structured grid generated inviscid flow solver.

One such structured grid inviscid code is BLUNT2D which is a time-dependent solution for axisymmetric flow over a blunt body that was developed by H. Harris Hamilton and John R. Spall in 1986¹⁵. The typical run-times of BLUNT2D are on the order of a few minutes.

LATCH and UNLATCH:

Langley Approximate Three-dimensional Convective Heating (LATCH) code was developed to compute viscous solutions using single block structured grids^{16,17}. As an extension to this code using unstructured grids, Hamilton et al. created a viscous code solver called UNLATCH that, when used in conjunction with a full three-dimensional, inviscid flowfield solution, rapidly computes convective heating rates that compare with N-S solutions^{3,4}.

LATCH and UNLATCH are based on the axisymmetric analog for general three-dimensional boundary layers. Axisymmetric analog assumes that the viscous crossflow in the boundary layer is small and can be neglected, thus, reducing the three-

dimensional boundary-layer equations to the same form as the axisymmetric boundary-layer equations¹⁸. Therefore, the heating on a three-dimensional body is computed along inviscid surface streamlines by replacing the radius of the axisymmetric body with the metric coefficient that is related to the converging or diverging of the surface streamlines. UNLATCH is also capable of computing finite catalytic wall effects on heating using an approximate method developed by Dr. George Inger¹⁹.

One such inviscid flow solver commonly used in conjunction with UNLATCH is CART3D, which is a finite volume based flow solver originally created for subsonic/transonic flight regime, but has since been extended to the hypersonic flight regime¹⁶. Using these applications, a typical solution for both laminar and turbulent flow can be computed in approximately 15-30 minutes, depending on the complexity of the vehicle's mesh.

3.2.3 Interpolation Programs

Grant Palmer has developed a program titled Automated Design Space Interpolation (ADSI) code to interpolate a database of surface solutions to a point in the trajectory space^{5,6}. ADSI performs a series of complex interpolation schemes in a one-, two-, or three-dimensional trajectory space. Once the database is populated, ADSI performs very efficient calculations with acceptable accuracy. However, ADSI requires a fair number of database solutions and does not consider mathematical relationships that exist between the interpolated variables.

3.3 Analytical Solutions

Analytical solutions to calculate heat flux have been developed by studying how heat transfer rates vary with given freestream conditions. Though lofty, the goal with analytical analysis is to develop simple heating equations that can be used to quickly compute heating rates for various vehicle shapes and configurations. This type of a solution may seem unattainable, but a number of heating relations for various conditions and configurations have been successfully developed and are summarized below.

3.3.1 Fay and Riddell

In 1957, Fay and Riddell²⁰ carried out a rigorous study of stagnation heat transfer, $q_{w,s}$, at hypersonic speeds which resulted in the following expression for equilibrium boundary layer:

$$q_{w,s} = 0.57 \left(\frac{4}{3}\right)^j Pr^{-0.6} (\rho_e \mu_e)^{0.4} (\rho_w \mu_w)^{0.1} \sqrt{\left(\frac{du_e}{dx}\right)} (h_0 - h_w) \left[1 - (Le^{0.52} - 1) \left(\frac{h_D}{h_0}\right) \right] \quad (3.1)$$

where: $j=0$ for two-dimensional flow and $j=1$ for axisymmetric flow.

The term in the square bracket, which accounts for the contribution of chemical reactions, is approximately 1.0 for binary mixtures, such as air, so it can safely be neglected in preliminary analysis¹⁰. As noted by Anderson⁹, Fay and Riddell's analysis covered a range of velocities from 5800 to 22,800 ft/s and wall temperatures from 300 to 3000 K (540 to 5400 °R). Remarkably, Fay and Riddell's equation is still considered today to be the most accurate method to calculate the stagnation heat transfer rate.

Another similar equation given by Van Driest in 1956²¹ prior to Fay and Riddell is the following.

$$q_{w,s} = 0.763 Pr^{-0.6} (\rho_e \mu_e)^{0.5} \sqrt{\left(\frac{du_e}{dx}\right)} (h_0 - h_w) \quad (3.2)$$

Equation 3.2 applies to the stagnation point of a sphere in equilibrium. It is similar to the axisymmetric version of Fay and Riddell's equation except it does not account for chemical reactions and the often difficult to predict density and viscosity wall properties are not required.

3.3.2 Generalized Heating Equations

Generalized aerodynamic heating relations have been developed and verified for the stagnation point of a transatmospheric vehicle and for laminar and turbulent flow over a

flat-plate at an angle-of-attack²². These heating equations take the form of the following expression⁹:

$$q_w = \rho_\infty^N V_\infty^M C \quad (3.3)$$

where: N & S – exponential constants

C – constant specific to geometry

The coefficients in Equation 3.3 are given as the following. (Note: the C values are derived to work only with SI base units, and the resultant units of q_w are W/cm².)

Stagnation point flow:

$$\begin{aligned} N &= 0.5 \\ M &= 3 \\ C &= 1.83e - 8 \cdot R_N^{-0.5} \cdot \left(1 - \frac{h_w}{h_0}\right) \end{aligned} \quad (3.4)$$

Laminar flow over a flat plate:

$$\begin{aligned} N &= 0.5 \\ M &= 3.2 \\ C &= 2.53e - 9 \cdot (\cos(\alpha))^{0.5} \cdot \sin(\alpha) \cdot x^{-0.5} \cdot \left(1 - \frac{h_w}{h_0}\right) \end{aligned} \quad (3.5)$$

Turbulent flow over a flat plate:

$$\begin{aligned} N &= 0.8 \\ \text{with : } V_\infty &\leq 3962 \text{ m/s} \\ M &= 3.37 \\ C &= 3.89e - 8 \cdot (\cos(\alpha))^{1.78} (\sin(\alpha))^{1.6} x_T^{-0.2} \left(\frac{T_w}{556}\right)^{-0.25} \left(1 - 1.11 \frac{h_w}{h_0}\right) \end{aligned} \quad (3.6)$$

$$\begin{aligned} \text{with : } V_\infty &> 3962 \text{ m/s} \\ M &= 3.7 \\ C &= 2.2e - 9 \cdot (\cos(\alpha))^{2.08} (\sin(\alpha))^{1.6} x_T^{-0.2} \left(1 - 1.11 \frac{h_w}{h_0}\right) \end{aligned} \quad (3.7)$$

Additionally, there is an alternative value for the coefficient of C in Equation 3.4 to calculate the heating rating in Earth's atmosphere given by Sutton-Graves²³ that assumes $h_w/h_0 \ll 1$, the so called *very cold wall approximation*:

$$C = 1.74153 \times 10^{-8} \cdot R_N^{-0.5} \quad (3.8)$$

Chapter 4

Requirements and Considerations

When developing xTRAP, it was advantageous to follow the engineering design process of first defining user requirements and then outlining conceptual design considerations.

4.1 Requirements

The objective is to develop a program that that can rapidly predict convective heating rates at a given point along a transatmospheric trajectory over the entire surface of a vehicle which will be beneficial to the preliminary design of reentry vehicles. In order to meet this objective the following user requirements were developed and categorized under the main concerns of function, accuracy, efficiency and ease of use (Table 4.1).

Table 4.1 - User Requirements

#	Category	Requirement
1	Function	The program predicts the convective heating rate at any given point along the vehicle's body.
2	Function	The solution will vary with changes to altitude, freestream velocity and angle-of-attack.
3	Function	The program functions over a range of freestream velocities of 10,000 to 22,000 ft/s and an angle-of-attack of 25 to 45°.
4	Function	The altitude can vary +/- 10% from the baseline trajectory.

Table 4.1 Continued

#	Category	Requirement
5	Function	The tool can predict both laminar and turbulent heating.
6	Efficiency	Solutions must be computed within 15 seconds under the processing of a typical desktop computer.
7	Efficiency	The amount of time required to populate the database must be kept within two days for any given vehicle geometry.
8	Accuracy	Results must be no more than +/-15% off from the actual data that could be computed from the program that supplied the data.
9	Ease of Use	Must be developed on a commonly used software platform.
10	Ease of Use	Users should be able to easily modify the program as needed for different trajectories and vehicle geometries.

4.1.1 Function

The purpose of developing this program is to predict convective heating rates over the surface of a vehicle during a reentry trajectory. Interpolation will occur among known data points varying with altitude, freestream velocity and angle-of-attack. Therefore, the database tool must show the effects of changing the altitude, freestream velocity or angle-of-attack has on the resultant predicted heating rates.

The tool must operate over a freestream velocity range of 10,000 to 22,000 ft/s to cover the main areas of concern when considering aerothermal loading during entry into Earth's atmosphere. The range of angle-of-attack is chosen to ensure the program can predict heating rates for vehicles on lifting trajectories with a large angle-attack like that was used for the Space Shuttle. Also, in order to predict the affects to surface heating rates if the vehicle gets slightly higher or lower than the planned baseline trajectory, the altitude must be able to vary from 10% of the baseline trajectory. The tool should also predict both laminar and turbulent heating as stated in user requirement #5.

4.1.2 Efficiency

This program is being developed to aid in the preliminary design process of thermal protection systems. Therefore, the time required to compute the solution is essential and the accuracy of the results can be sacrificed to promote the efficiency. The efficiency is dependent on both the time required to populate the database and the time to execute the solution once the database has been populated. Both of these elements must be kept at a minimum to be a useful preliminary design tool.

In order to minimize the amount of time to populate the database, it is important to investigate what is the minimum number of known data points required to achieve the required accuracy (See Section 4.1.3). Since the majority of the time required to compute a solution will be consumed by first populating the database, keeping this number of known data points to a minimum will have the largest effect on efficiency. Once the database has been populated for a given vehicle's geometry then locations throughout the trajectory space can be selected to predict the new data without the need to re-populate the database. Therefore, reducing the time required to execute the solution (User Requirement #6) is also a concern.

4.1.3 Accuracy

The tool is only as accurate as the supplied data used to populate the database. If the supplied data is poor, then the extrapolated solutions will be poor, but if the supplied data is reasonably accurate then the resultant extrapolated data should be sufficiently accurate. If accuracy is the main concern, then the database can be populated with solutions given by Navier-Stokes code based solvers. However, since this is to be used during preliminary design, it is more practical to use a boundary layer solver that has shorter runtimes to calculate the heating rates to populate the database such as SABLE or UNLATCH (see Section 3.2.2).

This database tool uses multiple levels of interpolation and extrapolation, which will each add losses to the accuracy, so it is important to choose types of regression that will minimize these losses. The requirement has been set to ensure that the final solutions

have no more than 15% error. Critical locations throughout the flowfield will be chosen to compare the percent error between the predicted value resulting from this tool and the actual value that could be calculated using the program that generated the supplied data.

4.1.4 Ease of Use

In order for this tool to be regularly utilized, it must be user friendly and adaptable for many different applications. The database tool must be developed on a common software platform such as Microsoft Excel or Microsoft Access making it easy to share among users. The tool will be protected to ensure regular users do not make a change that is detrimental to the program but the password will be provided to allow advanced users to make changes as necessary. The user will be able to modify the baseline trajectory and supplied source data for different vehicle's geometry as needed.

4.2 Design Considerations

This tool predicts the heating rate per unit area along a vehicle based on interpolation between known solutions at a trajectory point and extrapolation of boundary layer correlations. The idea as tasked by H. Harris Hamilton²⁴ is to interpolate between angle-of-attacks at one point in the trajectory space and then use methods similar to those employed by Dr. Ron Merski²⁵ to predict the heating rates at other points throughout the trajectory space. To develop correlations for changing velocity, evenly spaced points along a baseline trajectory will be chosen and stored in the database. Additionally, to improve accuracy when extrapolating to locations off the baseline trajectory, data points at 10% higher and 10% lower than the baseline will be chosen at the same trajectory point that the solutions that vary with angle-of-attack are computed. Also, the data points will have to be computed for both laminar and turbulent heating to determine the heating specific to each flow profile. Once all these values are calculated, they will be stored in a database where they can be easily retrieved to predict the values at various other locations throughout the trajectory space.

4.2.1 Trajectory and Geometry

The baseline trajectory for this program should be chosen to represent a typical reentry trajectory of a vehicle similar to design and mission of the Space Shuttle. A typical mission of the Shuttle or any similar replacement vehicle would be to fly to the International Space Station in Low-Earth-Orbit (LEO), complete various experiments and then return safely to Earth. As mentioned in Section 2.1, the Shuttle performs a lifting entry with the velocity varying with altitude represented by Equation 2.1. However, the vehicles proposed to replace the Shuttle have geometries similar to the Apollo capsules so, their associated lift parameter would be higher than the Shuttle but they are expected to still perform a lifting entry. Therefore, for the purpose of this program, the standard atmosphere data, along with a lifting entry and a relatively high lift parameter, will be chosen to determine the baseline trajectory.

The geometry chosen for the entry vehicle of this program will be a blunt-nose body typical of many reentry vehicles. To simplify the program, an axisymmetric spherical nose cone is chosen so specific locations along the body can be defined by their surface distance from the nose.

4.2.2 Number of Data Points

As alluded to in Section 4.1.2, an important question that must be answered is how many data points will need to be calculated to populate the database and ensure reasonably accurate results. This is a difficult problem because of the multiple levels of interpolation incorporated into the solution. Data points must be interpolated between heating rates that vary with velocity, altitude and angle-of-attack while at each level of interpolation a minimum of two known data points are required to implement some form of interpolation. Also, a fully laminar and a fully turbulent solution must be calculated at each appropriate trajectory point in order to meet the user requirements. The number of required data points can quickly escalate so it is important to implement a precise form of interpolation that keeps this number to a minimum. In order to further analyze this question, the different methods of interpolation are outlined below.

4.2.3 Interpolation

By definition, *interpolation* is a method of constructing new data points within the range of a discrete set of known data points. In general, the process of determining a function that closely fits known data points is called *curve fitting* or *regression analysis*.

However, the drawback with implementing a regression fit over multiple data points is that the determined trend line does not necessarily pass through the known points.

However, interpolation is a specific type of curve fitting that ensures that the function goes exactly through the data points.

Linear Interpolation

The simplest form of interpolation is linear interpolation which assumes a straight line approximation between adjacent data points. Given two data points, (x_a, y_a) and (x_b, y_b) , the linear interpolation relation is given by:

$$y = y_a + (y_b - y_a) \frac{(x - x_a)}{(x_b - x_a)} \text{ at the point } (x, y) \quad (4.1)$$

The limitation of linear interpolation is that it is not very precise or smooth because it is piecewise linear and only depends on the adjacent data points, so knowing values of additional points do not improve the accuracy of the approximation.

Polynomial Interpolation

Polynomial interpolation is an extension of linear interpolation because it seeks to fit a higher order polynomial to the data points. Polynomial expressions of the following form are used to interpolate a value at point $(x, f(x))$ with coefficients A, B, C, D , etc.

representing curve fitting constants:

$$f(x) = A + Bx + Cx^2 + Dx^4 \dots \quad (4.2)$$

Polynomial interpolation improves the smoothness and precision of linear interpolation yet it has its own limitations, namely because it deals with higher order polynomials, it

tends to be a more complicated solution and it has the potential to create unwanted oscillations.

Spline Interpolation

Spline interpolation is similar to linear interpolation in that it creates piecewise segments between each adjacent data points but it typically fits low-order polynomial functions as opposed to linear piecewise functions. What makes spline interpolation unique is that the chosen low-order polynomial segments are several times differentiable so the solution is smooth and the unwanted oscillations of higher-order polynomial interpolation are eliminated²⁶. Spline interpolation is more difficult to compute than simple linear interpolation, but it is often easier to compute than high-order polynomial interpolation.

From a practical point of view, *cubic splines* are most commonly implemented. A cubic spline is a continuous function that has continuous first and second derivatives everywhere in the interval and in each subinterval of the partition, and is represented by a polynomial of degree three²⁶.

4.2.4 Extrapolation

Another important element to understand when developing this program is the concept of extrapolation. *Extrapolation* is a method to construct data points outside a discrete set of known data points. Compared to interpolation, extrapolation can be rather uncertain because it projects data past the boundaries of known data points.

Extrapolation assumes that a similar relation exists outside the data points as observed between the data points. Extrapolation methods can be linear, polynomial, spline, etc. but the use of polynomial or spline extrapolation can often cause large spikes in approximations so caution must be used when applying relations outside of known data points.

Extrapolation methods can become less risky if proven physics based expressions are used to project the data. In the case of this task, proven hypersonic approximations and boundary layer expressions will be used where appropriate to reduce the uncertainty caused by extrapolation. It is important to note that even physics based

extrapolation will often cause a greater percent error than using interpolation methods, but this relative error is tolerable because it will greatly reduce the number of data points needed to construct the solutions.

Chapter 5

Analysis and Design

This chapter details the procedure used to develop xTRAP and summarizes the final design.

5.1 Analysis

5.1.1 Extrapolation Procedure

xTRAP follows a procedure, as advised from H. Harris Hamilton, to approximate the convective heating rates in trajectory space²⁴. As previously mentioned, this procedure is adapted from a method used by Dr. R. Merski to extrapolate surface heating rates from a wind tunnel test model to flight conditions²⁵. This procedure is applicable to approximate the surface heating rate in trajectory space for a single point on a three-dimensional body at an angle-of-attack. However, to simplify the description and the computational time required to generate source data, the procedure has been applied to an axisymmetric spherically blunted cone at zero angle-of-attack. As such, different cone half-angles will replace angles-of-attack in this analysis and discussion because changing either of these elements has the same effect on the heating along a body²⁴.

xTRAP applies this procedure numerous times to predict the surface heating at various points along a body at a given point in the trajectory space defined by altitude and freestream velocity. Freestream conditions and angle-of-attack can be quickly changed when needed to predict the heat transfer rates along the entire trajectory.

Assume the cone enters an atmosphere on the lifting entry trajectory shown in Figure 5.1. If a database of known solutions consist of the following:

1. Heating solutions computed at the mid-freestream velocity over a range of cone half-angles, on the baseline trajectory and at specified altitudes above and below the baseline altitude (indicated by diamond shape in Fig. 5.1), and
2. Inviscid velocity solutions computed at regular intervals along the baseline trajectory (indicated by 'X' in Fig. 5.1).

Then, the following procedure can be used to extrapolate heating solutions to various other points within the defined trajectory space shown.

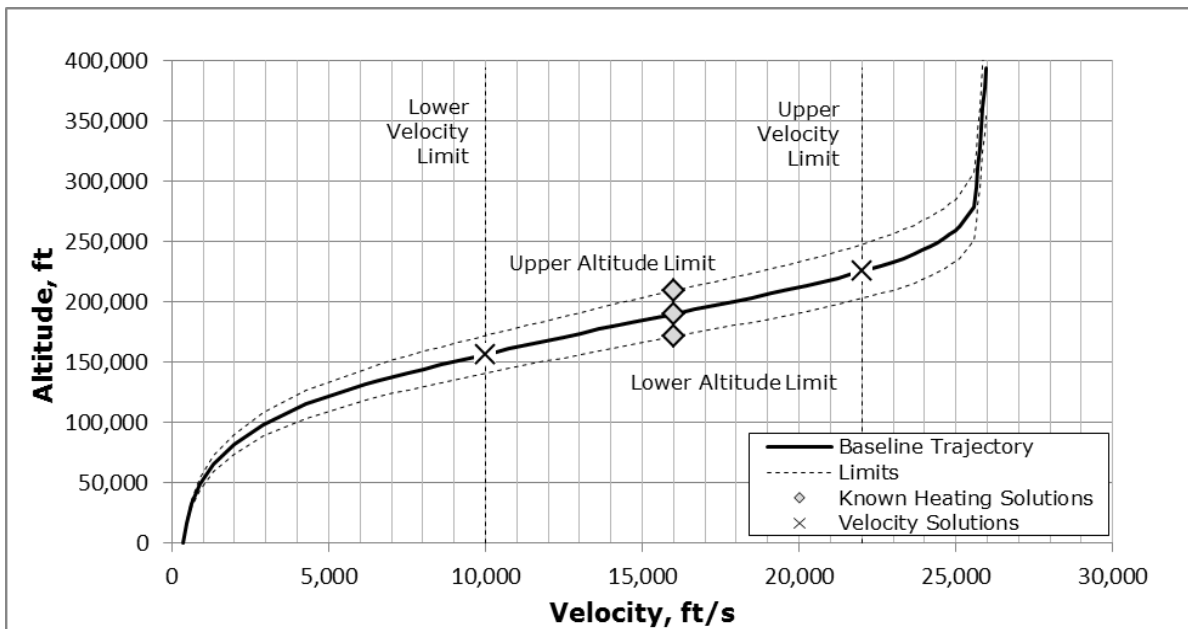


Figure 5.1 - Baseline Trajectory with Deviation Limits

(lift parameter = 733 kg/m^2 (4.67 slugs/ft^2))

The extrapolation procedure relies on the following principle which relates the heat transfer coefficient for a position along the body to the heat transfer coefficient at the stagnation point for laminar flow:

$$\frac{h_{cf}}{h_{cf,s}} \approx \text{constant} \quad (5.1)$$

This statement is valid because both h_{cf} and $h_{cf,s}$ have the same functional dependence on Reynolds number²⁴. Mathematically, Equation 5.1 can also be expressed by the following equation comparing Point 2 to Point 1 in the trajectory space with X representing an extrapolation factor.

$$\left[\frac{h_{cf}}{h_{cf,s}} \right]_2 = \left[\frac{h_{cf}}{h_{cf,s}} \right]_1 X \quad (5.2)$$

From Equation 5.2, if the heat transfer coefficients are known at Point 1 ($[h_{cf}/h_{cf,s}]_1$) and the stagnation point heat transfer coefficient can be calculated at Point 2 ($h_{cf,sr2}$), then the following equation can be used to calculate the heat transfer coefficient at Point 2 ($h_{cf,2}$) if an appropriate X value is determined.

$$h_{cf,2} = h_{cf,sr2} \left[\frac{h_{cf}}{h_{cf,s}} \right]_1 X \quad (5.3)$$

(Note: Adding the X value expands this formula to be used for turbulent flow extrapolations, see Section 5.1.4) Then, from knowing the value of $h_{cf,2}$, the heating rate at the wall, $q_{w,2}$ can be determined by the following equation:

$$q_{w,2} = h_{cf,2} (h_{aw,2} - h_{w,2}) \quad (5.4)$$

This is the basic method of extrapolation used to develop xTRAP. However, the following details are needed to understand how to utilize these equations.

5.1.2 Known and Unknown Points

The database solutions computed at the midway point of the freestream velocity range (at $V_\infty=16,000$ in Figure 5.1) are represented by the subscript 1. These solutions share the same freestream velocity but are computed for various altitudes and cone-half angles. Together all the solutions at this location are considered *Point 1* in this analysis. The extrapolated point, *Point 2*, represented by the subscript 2, is the location in the

trajectory space where the solution is not yet known. Point 1 values are interpolated based on values specified by the user for Point 2's configuration and location before the data is extrapolated to a new location. Specifically, the user specified angle-of-attack determines the appropriate cone-half angle solution to be used at Point 1 and the altitude specified by the user for Point 2 determines the percent above or below the baseline altitude used for Point 1.

The following figures show how the heating rate changes with cone-half angle and altitude, respectively (Fig. 5.2 and 5.3).

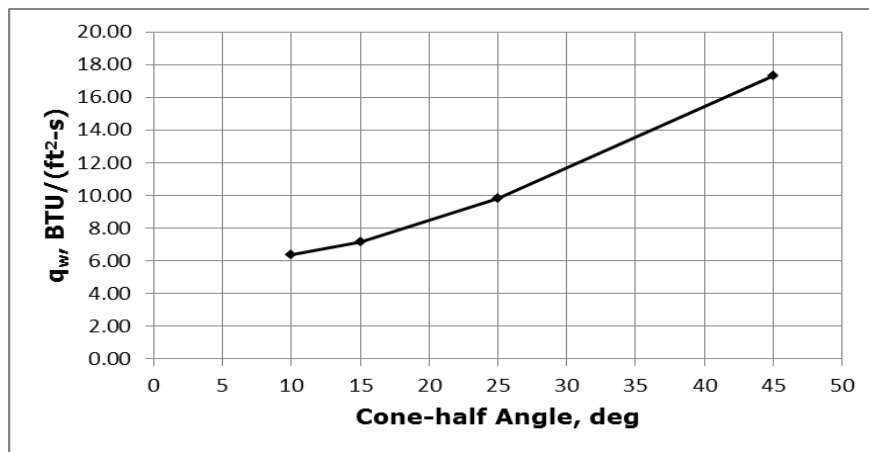


Figure 5.2 - Effects of Varying Cone-half Angle on Heating Rates

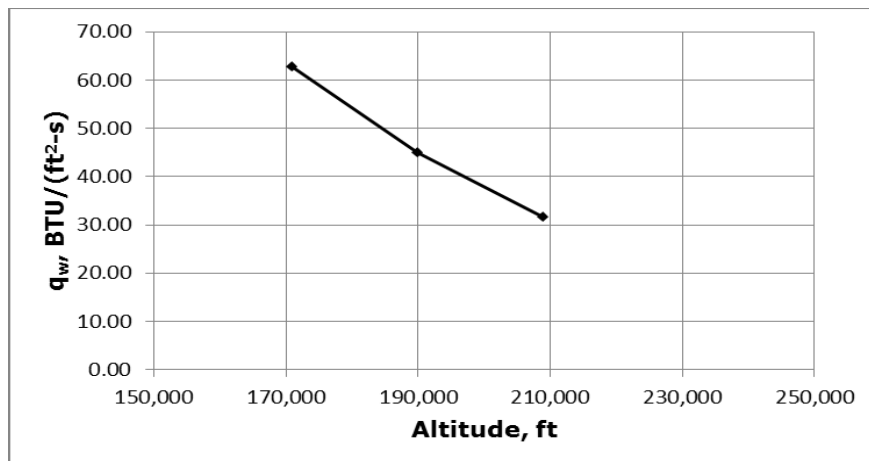


Figure 5.3 - Effects of Varying Altitude on Heating Rates

5.1.3 Extrapolation Terms

Instead of working with heating rates, q_w , directly, this procedure deals with heat transfer coefficients because heat transfer coefficients are relatively insensitive to wall temperature²⁴. The following defines the heat transfer coefficient:

$$h_{cf} = \frac{q_w}{(h_{aw} - h_w)} \quad (5.5)$$

The adiabatic wall enthalpy, h_{aw} , is calculated by the following:

$$h_{aw} = h_e + r \left(\frac{u_e^2}{2} \right) \quad (5.6)$$

where r is the recovery factor which is approximately equal to the following for laminar and turbulent flow, respectively.

$$r_L \approx \sqrt{Pr} \quad (5.7)$$

$$r_T \approx \sqrt[3]{Pr} \quad (5.8)$$

The wall enthalpy, h_w , is determined based on knowing the thermodynamic properties at the wall. In the case of computing solutions using the boundary layer code SABLE (see Section 3.2.2), the wall temperature and pressure at the edge of the boundary layer are given in the outputted data file. If the database solutions are computed for perfect gas then the following equation can be used to calculate wall enthalpy.

$$h_w = C_p T_w \quad (5.9)$$

However, if the database solutions are computed for equilibrium air chemistry, such as used in xTRAP, one must look-up the wall enthalpy based on knowing two thermodynamic properties (T_w and p_e) because the pressure does not change in the normal direction throughout the boundary layer (Eq. 5.10).

$$p_w = p_e \quad (5.10)$$

In order to apply Equation 5.4, Equation 5.6 is used to determine h_{aw} and two thermodynamic properties are used to determine h_w . However, the local properties at the edge of the boundary layer are first needed to determine h_e in Equation 5.6 and to determine one of the wall properties based on Equation 5.10. The non-dimensional ratio of the boundary layer edge pressure to the freestream dynamic pressure has been found to correlate the local pressure reasonably well (Eq. 5.11).

$$\left(\frac{p_e}{\frac{1}{2} \rho_\infty V_\infty^2} \right) \approx \text{constant} \quad (5.11)$$

Therefore, the edge pressure can be approximated by the following:

$$p_{e,2} \approx (\rho_\infty V_\infty^2)_2 \left(\frac{p_e}{\rho_\infty V_\infty^2} \right)_1 \quad (5.12)$$

When determining the u_e term in Equation 5.6, it was noted that a non-dimensional velocity term (u_e^2/V_∞^2) does not correlate like the pressure. Therefore, a correction factor for the velocity, CF_{ue} , can be added for the correlation in the following form:

$$u_{e,2} = \sqrt{V_{\infty,2}^2 \left(\frac{u_e^2}{V_e^2} \right)_1} CF_{ue} \quad (5.13)$$

The correction factor, CF_{ue} , can be determined by interpolating the non-dimensional velocity ratio for Point 2 over Point 1 with respect to changing freestream velocity. This is why solutions along the baseline trajectory are required to be stored in the database. As shown in Figure 5.4, this velocity ratio will decrease with increasing velocity.

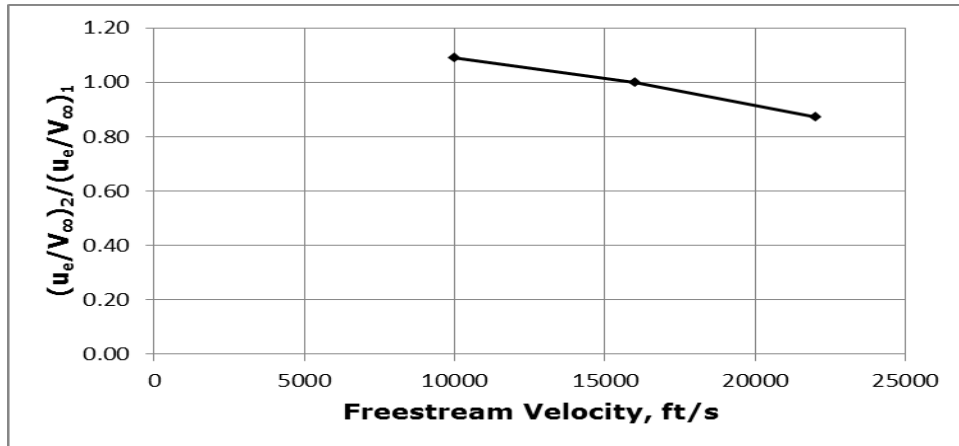


Figure 5.4 - Typical Velocity Correlation

Once the edge velocity is calculated, the edge enthalpy is calculated from Equation 5.14 with the total enthalpy defined in Equation 5.15.

$$h_{e,2} = h_{0,2} - \frac{u_e^2}{2} \quad (5.14)$$

$$h_0 = h_\infty + \frac{u_\infty^2}{2} \quad (5.15)$$

Now both p_e and h_e are known so other thermodynamic properties such as T_e and ρ_e can be looked up in equilibrium air tables.

The only remaining Point 2 parameter needed to apply Equation 5.4 is a value for the wall temperature. If $T_{w,2}$ was known, then $h_{w,2}$ of Equation 5.4 can be determined by looking up in equilibrium air tables since $p_{w,2}$ is already known. However, if $T_{w,2}$ is not known, the radiative equilibrium wall condition can be applied to solve this temperature. This is a condition when the convective heat transfer to the wall is equal to the radiative heat transfer away from the wall, represented in the following equation:

$$q_w = q_{RS} \quad (5.16)$$

The radiative surface heat transfer rate, q_{RS} , is defined by the following formula, with ε representing the surface emissivity (approximated at 0.9) and σ the Stefan-Boltzmann constant ($4.761\text{e-}13 \text{ BTU}/(\text{ft}^2\text{-s-}^\circ\text{R}^4)$):

$$q_{RS} = \varepsilon \sigma T_w^4 \quad (5.17)$$

Then, set the right side of Equation 5.4 equal to the right side of Equation 4.16 and solve for $T_{w,2}$ as shown below:

$$h_{cf,2}(h_{aw,2} - h_{w,2}) = \varepsilon \sigma T_{w,2}^4 \quad (5.18)$$

Since $h_{w,2}$ is dependent of T_w this equation must be solved iteratively. Once this value is solved, everything required to complete the extrapolation is known, assuming the stagnation heating rate can be calculated, and an appropriate value for the extrapolation factors can be approximated for both laminar and turbulent flow.

5.1.4 Stagnation Heating

Fay and Riddell's equation (Eq. 3.1) was chosen to determine the stagnation heating rates, $q_{w,s}$, for Point 1 and Point 2 which were then converted to heat transfer coefficients based on Equation 5.5. Simpler methods such as Van Driest's equation (Eq. 3.2) and Sutton-Graves' generalized equation (Eq. 3.8) were also used in developing xTRAP, but, as expected, the Fay and Riddell method proved to be most accurate. The du_e/dx term in Equation 3.1 was obtained from the modified Newtonian theory as the following:

$$\frac{du_e}{dx} = \frac{1}{R_N} \left[\frac{2(p_e - p_\infty)}{\rho_e} \right]^{\frac{1}{2}} \quad (5.19)$$

Therefore, the Fay and Riddell formula took the following form:

$$q_{w,s} = 0.76 Pr^{-0.6} (\rho_e \mu_e)^{0.4} (\rho_w \mu_w)^{0.1} \left[\frac{2(p_e - p_\infty)}{\rho_e} \right]^{\frac{1}{4}} \frac{h_0}{\sqrt{R_N}} \left(1 - \frac{h_w}{h_0} \right) \quad (5.20)$$

The total enthalpy was calculated from Equation 5.15 and the nose radius was given by the cone's geometry. The density at the edge of the boundary layer was determined by looking in equilibrium air tables and knowing the edge pressure and enthalpy from Equation 5.12 and 5.14, respectively. The wall enthalpy and density was looked up in equilibrium tables after iteratively determining the wall temperature from Equation 5.18 and knowing the wall pressure from Equation 5.10. The edge and wall viscosities shown in Equation 5.20 were calculated based on *Sutherland's Law*⁹. Sutherland's Law says for a pure, non-reacting gas, the viscosity coefficient is dependent only on temperature by the following relationship:

$$\frac{\mu}{\mu_{ref}} = \left(\frac{T}{T_{ref}} \right)^{\frac{3}{2}} \left(\frac{T_{ref} + S}{T + S} \right) \quad (5.21)$$

Where²⁸:

$$\begin{aligned} \mu_{ref} &= 1.789e - 5 \text{ kg / m s} \\ T_{ref} &= 273.1 \text{ K} \\ S &= 110.6 \text{ K} \end{aligned}$$

5.1.5 Extrapolation Factors

As implied in Section 5.1.1 the extrapolation factor of Equation 5.3 is approximately equal to unity for laminar flow. However, the extrapolation factor for turbulent flow is not as simple. Merski looked at heat transfer rate correlations reported by Tauber and Meneses²² to develop his extrapolation factors to relate his wind tunnel model data to flight conditions²⁵. These derivations are outlined below and they form the basis for the extrapolation values implemented in xTRAP.

Similar to the generalized heating equations (see Section 3.3.2), the local heat transfer coefficient at the stagnation point of a sphere is the following:

$$h_{cf,s} = \rho_{\infty}^{0.5} V_{\infty}^3 \left(\frac{R_c}{L} \right)^{-0.5} L^{-0.5} \frac{A_s}{h_0} \quad (5.22)$$

where L is the length of the geometry and A is a constant dependent on angle-of-attack and geometry considerations. Likewise, the heat transfer coefficient for a laminar flat-plate is the following:

$$h_{cf,L} = \rho_{\infty}^{0.5} V_{\infty}^{3.2} \left(\frac{\xi}{L} \right)^{-0.5} L^{-0.5} \frac{A_L}{h_0} \quad (5.23)$$

where ξ is the running length from the start of the streamline. For turbulent flow, Merski listed the following correlation:

$$h_{cf,T} = \rho_{\infty}^{0.8} V_{\infty}^{3.37} \left(\frac{\xi}{L} \right)^{-0.2} L^{-0.2} T_w^{-0.25} \frac{A_T}{h_0} \quad (5.24)$$

where ξ is the running length from the start of transition. However, according to the other form of the generalized heating equation for turbulent flow, given in Section 3.3.2 (Eq. 3.7), an alternative form of the heat transfer coefficient for turbulent flow can be derived as the following:

$$h_{cf,T} = \rho_{\infty}^{0.8} V_{\infty}^{3.7} \left(\frac{\xi}{L} \right)^{-0.2} L^{-0.2} \frac{A_T}{h_0} \quad (5.25)$$

Based on these correlations, extrapolation factors for laminar and turbulent flow can now be determined by dividing the local laminar or turbulent enthalpy, h_{cf} (Eq. 5.23 and 5.24/5.25, respectively) by the stagnation point enthalpy, $h_{cf,s}$ (Eq. 5.20). From rearranging Equation 5.2, the laminar and turbulent flow extrapolations are defined by the following:

$$X_L = \frac{\left(\frac{h_{cf,L}}{h_{cf,s}} \right)_2}{\left(\frac{h_{cf,L}}{h_{cf,s}} \right)_1} \quad (5.26)$$

$$X_T = \frac{\left(\frac{h_{cf,T}}{h_{cf,s}} \right)_2}{\left(\frac{h_{cf,T}}{h_{cf,s}} \right)_1} \quad (5.27)$$

So, if Equations 5.22, 5.23, 5.24 and 5.25 are substituted into Equations 5.26 and 5.27 and cancelations are made for running lengths, ξ , and the constants, A , the extrapolation factors result in the following:

$$X_L = \left(\frac{V_{\infty,2}}{V_{\infty,1}} \right)^{0.2} \quad (5.28)$$

$$X_T = \left(\frac{\rho_{\infty,2}}{\rho_{\infty,1}} \right)^{0.3} \left(\frac{V_{\infty,2}}{V_{\infty,1}} \right)^{0.37} \left(\frac{L_2}{L_1} \right)^{0.3} \left(\frac{T_{w,2}}{T_{w,1}} \right)^{-0.25} \quad (5.29)$$

$$X_T = \left(\frac{\rho_{\infty,2}}{\rho_{\infty,1}} \right)^{0.3} \left(\frac{V_{\infty,2}}{V_{\infty,1}} \right)^{0.7} \left(\frac{L_2}{L_1} \right)^{0.3} \quad (5.30)$$

As said, the laminar extrapolation factor is approximately unity, but the value given in Equation 5.28 was preferred in developing xTRAP because it was found to give better results. According to the freestream velocity associated with Equation 3.7, the turbulent extrapolation factor derived by Merski in Equation 5.29 would best apply when freestream velocities are below 13,000 ft/s. However, at higher freestream velocities Equation 5.30 should provide better results for extrapolating turbulent flow data. In the case of xTRAP, the freestream velocity of Point 1 is at 16,000 ft/s, so it was found to be more accurate to implement a form of Equation 5.30 when extrapolating data using

xTRAP. xTRAP does have the ability to extrapolate parameters to freestream velocities below 13,000 ft/s but Equation 5.30 was still found to give better results than Equation 5.29 because the dominating effects of Point 1.

The turbulent extrapolation factors are somewhat more complicated than the laminar results, but based on results of xTRAP, Equation 5.30 has been simplified to the following:

$$X_T = \left(\frac{\rho_{\infty,2}}{\rho_{\infty,1}} \right)^{0.3} \left(\frac{V_{\infty,2}}{V_{\infty,1}} \right)^{0.7} \quad (5.31)$$

Dropping the ratio of geometry length, L , in Equation 5.30 can easily be justified for the case of xTRAP because the size and shape of the vehicle's body does not change between Point 1 and Point 2.

5.2 Design

The following information details the design of the various components of xTRAP.

5.2.1 Database and CFD Solutions

In order to easily store and manipulate large amounts of heating data, Microsoft (MS) Excel was chosen to develop this extrapolation tool. Recent versions of MS Excel do not have the data restrictions of previous versions and it provides many numerical analysis functions that are not as easily implemented using a database program such as Microsoft Access. Microsoft Excel was also chosen because it is well known in industry and it allows algorithms, such as cubic splines algorithms, to be easily added for interpolation applications.

The CFD solutions that were computed and stored in the database were generated using the boundary layer code, SABLE, and the inviscid flow solver, BLUNT2D. The various data points were run in equilibrium air conditions because it is considered more accurate

than perfect gas assumptions in the range of Mach numbers considered (approximately Mach 10 to Mach 22). After running the BLUNT2D inviscid solution the SABLE code was run for both laminar and turbulent flow, and the data from the output file were copied as text into the MS Excel database.

5.2.2 Trajectory and Geometry

The baseline trajectory was calculated by listing U.S. Standard Atmosphere, 1976²⁹ data at 5000 meter altitude increments from 0 to 40 km and 80 to 120 km and 1000 meter increments from 40 to 80 km. The atmospheric densities were then used in the lifting entry equation (Eq. 2.1) with a radius of curvature of 6.39e6 meters and a lift parameter of 733 kg/m². These numbers can be adjusted as needed but were chosen to represent a lifting body entry vehicle returning from LEO with a lift-to-drag ratio lower than the Space Shuttle.

As advised, a blunted sphere nose cone was used for the vehicle's body. The cone has a one-to-seven ratio of nose radius to body length. The results were analyzed based on a nose radius of 2 feet and body length of 14 feet. The cone-half angle ranged from 10 to 45 degrees to analyze the effects of changing angle-of-attack. The solutions computed along the baseline trajectory were at a cone-half angle of 25 degrees which is near midway between the angles of interest.

5.2.3 Interpolation and Extrapolation

A Visual Basics Application algorithm (Appendix A) was written based on common codes available on the internet and added to the Excel program to determine cubic spline interpolation. Once the algorithm was added, the implementation of cubic splines was actually easier than basic linear interpolation, so the use of cubic spline interpolation is preferred anytime the curve fit would be perceived different from a linear function. Therefore, cubic splines are utilized when reading the SABLE output data and when interpolating between cone-half angles, altitudes and velocities. The only time a linear interpolation method is utilized is when the program interpolates freestream temperatures. This is because a plot of standard atmosphere temperature shows large

isothermal or gradient temperatures regions, which are piecewise linear segments characteristic of linear interpolation.

Extrapolation methods are used to project results from 16,000 ft/s to other points within the defined trajectory space. However, the observed trend data between known points are not simply extended to other points outside the known data points. Instead, the heating data is extrapolated based on known hypersonic and boundary layer theory as detailed in Section 5.1.

5.2.4 Number of Data Points

The following data points were computed and stored in the database in order to analyze the accuracy over the range of freestream velocities specified in Table 4.1 (10,000 to 22,000 ft/s). Four data points at cone-half angles 10° , 15° , 25° and 45° were computed on the baseline at 16,000 ft/s to account for changing angle-of-attack. To improve the results when the vehicle strayed higher or lower than the baseline trajectory, four data points were also computed at angles 10° , 15° , 25° and 45° at 10% higher than the baseline altitude at 16,000 ft/s and four more points were computed at angles 10° , 15° , 25° and 45° at 10% lower than the baseline altitude at 16,000 ft/s. Two additional 25° cone-half angle data points at 10,000 and 22,000 ft/s along the baseline trajectory were computed to correlate velocities. Including both laminar and turbulent solutions at each of the data points at 16,000 ft/s, but not along the other baseline points, made the total number of data points equal 26.

Investigations were made to improve accuracy within this range of freestream velocities and to extend the results below 10,000 ft/s or above 22,000 ft/s. The results were validated against the supplied SABLE data to determine percent error accuracy. The lessons learned from these investigations were incorporated in the development of xTRAP. The limits tell the user which specific data points are needed when setting up the database to ensure a given accuracy over a given range of velocities. A summary of these results are listed Section 6.2.

5.2.5 Operating xTRAP

A detailed user manual for xTRAP will be developed in a separate document. However, this section summarizes the main steps required to run a solution. (see Appendix B showing a screen shoot of xTRAP for reference.)

The steps required to operate xTRAP are to 1) complete the initial setup, 2) add source data, and 3) select the trajectory point where the solution is desired to be determined. The initial setup of xTRAP requires selecting the fluid flow profile (fully laminar, fully turbulent or transition), maximum percent error, allowable altitude deviations, angle-of-attacks of interest and a range of freestream velocities. Also, the user at this point confirms the baseline trajectory data is adequate or adjusts accordingly. With this information provided, xTRAP determines what data points need to be computed and stored in the database, and then outputs the total number of required data points. The user then enters the required source data and confirms that this source data has been supplied. The final steps are to enter the freestream conditions and angle-of-attack to define the new trajectory point and then select the desired output parameter and positions along the body (surface distance from stagnation point, s). Additionally, the user selects a transition point along the body. Body positions selected higher than this transition point will be turbulent and positions lower will be laminar.

Once these steps are complete, the user selects the "Calculate" button to compute the solution. The results of xTRAP are outputted within seconds. xTRAP has been developed to analyze up to 10 points along the body at a time so if more points are needed multiple runs are required. The user can choose to compare the data against additional data if the additional data is stored in the appropriate location in the database file. More details regarding this feature and other functions will be detailed in the user manual.

5.2.6 Resultant Data

Along with the required surface heat transfer rates, q_w , xTRAP can output various other aerothermal parameters used when calculating heating rates. These parameters are pressure, velocity and enthalpy at the edge of the boundary layer (p_e , u_e , h_e) and

temperature and enthalpy at the wall (T_w , h_w). Additional parameters are the adiabatic wall enthalpy (h_{aw}) and the heat transfer coefficient (h_{cf}). These parameters could also be useful for development of hypersonic vehicles, however, the accuracies of these variables have not been determined.

Chapter 6

Validation and Results

This chapter details the testing methods, presents the results, and evaluates how xTRAP performed at meeting the defined user requirements (Table 4.1).

6.1 Validation

6.1.1 Functional Testing

The following test cases were developed and executed to verify the basic functions of xTRAP. (Table 6.1).

Table 6.1 - Functional Testing

No.	Variable	Expected Results	Actual Results
<i>Note:</i> The following results compare with laminar heating rates measured at 3 feet from the stagnation point along a 25-degree half-angle blunted cone. The cone is at a trajectory point located at 16,000 ft/s and 190,000 ft.			
1	Increase freestream velocity to 19,000 ft/s.	q_w increases	q_w increases
2	Decrease freestream velocity to 13,000 ft/s.	q_w decreases	q_w decreases
3	Increase altitude to 209,000 ft.	q_w decreases	q_w decreases
4	Decrease altitude to 171,000 ft.	q_w increases	q_w increases

Table 6.1 Continued

No.	Variable	Expected Results	Actual Results
5	Increase cone-half angle to 45°.	q_w increases	q_w increases
6	Increase cone-half angle to 10°.	q_w decreases	q_w decreases
7	Change to fully turbulent flow.	q_w increases	q_w increases

Based on the results shown in Table 6.1, xTRAP functions as intended during basic operation. However, in order to determine how accurate xTRAP functions, extrapolated results have been plotted and validated against SABLE results (See Section 6.2 for details).

6.1.2 Verification of Requirements

After the development of xTRAP, the design was verified against the stated requirements listed in Table 4.1.

Table 6.2 - Verification of Requirements

#	Requirement	Requirement Met (Yes/No)? / Comments
1	The program predicts the convective heating rate at any given point along the vehicle's body.	Yes, predictions can be made at any user specified location.
2	The solution will vary with changes to altitude, freestream velocity and angle-of-attack.	Yes, as shown in Table 6.1.
3	The program functions over a range of freestream velocities of 10,000 to 22,000 ft/s and an angle-of-attack of 25 to 45°.	Yes, but can be extended to 6,000 ft/s and 24,000 ft/s and down to 10° angle-of-attack in other circumstances (see Section 6.2.2).

Table 6.2 Continued

#	Requirement	Requirement Met (Yes/No)? / Comments
4	The altitude can vary +/- 10% from the given trajectory.	Yes, as shown in Table 6.1.
5	The tool can predict both laminar and turbulent heating.	Yes, as shown in Table 6.1.
6	Solutions must be computed within 15 seconds under the processing of a typical desktop computer.	Yes, observed runtimes are no longer than 10 seconds on an Intel Duo Core 1.83 GHz processor.
7	The amount of time required to populate the database must be kept within two days for any given vehicle geometry.	Yes, in this case, 26 total data points at less than 30 minutes per point takes less than 13 hours.
8	Results must be no more than 15% off from the actual data that could be computed from the program that supplied the data.	No, not all results were less than 15% error. However, average results were less than 15% and operating ranges have been adjusted to ensure desired accuracy (see Section 6.2.2).
9	Must be developed on a commonly used software platform.	Yes, MS Excel was used.
10	Users should be able to easily modify the program as needed for different trajectories and vehicle geometries.	Yes, some cells are protected but the password can be provided.

Based on the results shown in Table 6.2, xTRAP meets the design requirements except more discussion is needed in regards to accuracy (see Section 6.2.2).

6.2 Results

Various points were chosen throughout the trajectory space to compare the accuracy of xTRAP. Since SABLE was used to populate the database, xTRAP is only as accurate as the source data supplied by SABLE. Therefore, percent error calculations were used to

compare the observed extrapolated results of xTRAP to the theoretical actual results using SABLE (Eq. 6.1).

$$\% \text{ error} = \left[\frac{(\text{xTRAP result}) - (\text{SABLE result})}{(\text{SABLE result})} \right] \times 100 \quad (6.1)$$

6.2.1 Accuracy and Plots

A summary of the tested scenarios are listed in the following tables (Table 6.3, 6.4, 6.5 and 6.5) showing maximum, minimum and average percent error values. Each scenario is also plotted in Appendix C, D, E and F as indicated. Plots show results in 0.5 foot increments from the stagnation point, 0 ft, to 14 ft along the surface of the body.

Table 6.3 - 25° Cone-half Angle Results

No.	Scenario	Percent Error		
		Max.	Min.	Ave.
Fig. C.1: Known Trajectory Points				
1.1	16,000 ft/s, 171,000 ft, laminar	0.0	0.0	0.0
1.2	16,000 ft/s, 171,000 ft, turbulent	0.0	0.0	0.0
1.3	16,000 ft/s, 190,000 ft, laminar	0.0	0.0	0.0
1.4	16,000 ft/s, 190,000 ft, turbulent	0.0	0.0	0.0
1.5	16,000 ft/s, 209,000 ft, laminar	0.1	0.0	0.0
1.6	16,000 ft/s, 209,000 ft, turbulent	0.1	0.0	0.0
Fig. C.2: Baseline Trajectory Points				
2.1	10,000 ft/s, 156,254 ft, laminar	12.4	-7.2	4.9
2.2	10,000 ft/s, 156,254 ft, turbulent	6.6	-12.5	-3.2

Figure 6.3 Continued

No.	Scenario	Percent Error		
		Max.	Min.	Ave.
Fig. C.2: Continued				
2.3	13,000 ft/s, 173,711 ft, laminar	8.0	-4.5	3.1
2.4	13,000 ft/s, 173,711 ft, turbulent	4.4	-5.5	0.2
2.5	19,000 ft/s, 206,158 ft, laminar	6.0	0.2	2.1
2.6	19,000 ft/s, 206,158 ft, turbulent	9.2	-2.7	5.2
2.7	22,000 ft/s, 225,254 ft, laminar	8.7	0.2	3.9
2.8	22,000 ft/s, 225,254 ft, turbulent	9.5	-7.4	1.4
Fig. C.3: 10% Above Baseline Trajectory Points				
3.1	10,000 ft/s, 171,880 ft, laminar	12.7	-7.6	4.9
3.2	10,000 ft/s, 171,880 ft, turbulent	6.9	-8.8	0.6
3.3	13,000 ft/s, 191,082 ft, laminar	7.8	-4.4	3.1
3.4	13,000 ft/s, 191,082 ft, turbulent	6.8	-2.9	2.3
3.5	19,000 ft/s, 226,774 ft, laminar	6.3	0.4	2.4
3.6	19,000 ft/s, 266,774 ft, turbulent	5.6	-4.6	1.1
3.7	22,000 ft/s, 247,779 ft, laminar	8.4	-0.2	3.8
3.8	22,000 ft/s, 247,779 ft, turbulent	-0.2	-17.8	-9.7
Fig. C.4: 10% Below Baseline Trajectory Points				
4.1	10,000 ft/s, 140,629 ft, laminar	11.8	-6.5	4.8
4.2	10,000 ft/s, 140,629 ft, turbulent	6.7	-14.0	-5.5
4.3	13,000 ft/s, 156,340 ft, laminar	7.7	-4.2	3.1
4.4	13,000 ft/s, 156,340 ft, turbulent	3.0	-6.4	-1.0

Figure 6.3 Continued

No.	Scenario	Percent Error		
		Max.	Min.	Ave.
Fig. C.4: Continued				
4.5	19,000 ft/s, 185,542 ft, laminar	5.6	0.0	1.7
4.6	19,000 ft/s, 185,542 ft, turbulent	12.3	-1.2	8.0
4.7	22,000 ft/s, 202,728 ft, laminar	7.2	-1.0	2.3
4.8	22,000 ft/s, 202,728 ft, turbulent	16.2	-5.5	8.4

Table 6.4 – 10° Cone-half Angle Results

No.	Scenario	Percent Error		
		Max.	Min.	Ave.
Fig. D.1: Known Trajectory Points				
1.1	16,000 ft/s, 171,000 ft, laminar flow	0.0	0.0	0.0
1.2	16,000 ft/s, 171,000 ft, turbulent flow	0.0	0.0	0.0
1.3	16,000 ft/s, 190,000 ft, laminar flow	0.0	0.0	0.0
1.4	16,000 ft/s, 190,000 ft, turbulent flow	0.0	0.0	0.0
1.5	16,000 ft/s, 209,000 ft, laminar flow	0.1	0.0	0.0
1.6	16,000 ft/s, 209,000 ft, turbulent flow	0.1	0.0	0.0
Fig. D.2: Lower and Upper Limit Trajectory Points				
2.1	10,000 ft/s, 140,629 ft, laminar	6.6	-17.4	-4.7
2.2	10,000 ft/s, 140,629 ft, turbulent	6.6	-25.7	-14.5
2.3	10,000 ft/s, 171,880 ft, laminar	6.4	-20.6	-6.0

Figure 6.4 Continued

No.	Scenario	Percent Error		
		Max.	Min.	Ave.
Fig. D.2: Continued				
2.4	10,000 ft/s, 171,880 ft, turbulent	6.4	-22.8	-9.2
2.5	22,000 ft/s, 202,728 ft, laminar	20.0	-1.0	9.5
2.6	22,000 ft/s, 202,728 ft, turbulent	27.7	-5.6	14.2
2.7	22,000 ft/s, 247,779 ft, laminar	22.3	-0.3	10.8
2.8	22,000 ft/s, 247,779 ft, turbulent	5.6	-18.0	-4.9

Table 6.5 - 45° Cone-half Angle Results

No.	Scenario	Percent Error		
		Max.	Min.	Ave.
Fig. E.1: Known Trajectory Points				
1.1	16,000 ft/s, 171,000 ft, laminar flow	0.0	0.0	0.0
1.2	16,000 ft/s, 171,000 ft, turbulent flow	0.0	0.0	0.0
1.3	16,000 ft/s, 190,000 ft, laminar flow	0.0	0.0	0.0
1.4	16,000 ft/s, 190,000 ft, turbulent flow	0.0	0.0	0.0
1.5	16,000 ft/s, 209,000 ft, laminar flow	0.0	0.0	0.0
1.6	16,000 ft/s, 209,000 ft, turbulent flow	0.1	0.0	0.0
Fig. E.2: Lower and Upper Limit Trajectory Points				
2.1	10,000 ft/s, 140,629 ft, laminar	6.9	2.0	4.0
2.2	10,000 ft/s, 140,629 ft, turbulent	6.9	-12.0	-7.8
2.3	10,000 ft/s, 171,880 ft, laminar	6.9	1.4	3.8

Figure 6.5 Continued

No.	Scenario	Percent Error		
		Max.	Min.	Ave.
Fig. E.2: Continued				
2.4	10,000 ft/s, 171,880 ft, turbulent	6.7	-6.9	-2.2
2.5	22,000 ft/s, 202,728 ft, laminar	2.7	-2.7	0.8
2.6	22,000 ft/s, 202,728 ft, turbulent	10.7	-5.6	6.5
2.7	22,000 ft/s, 247,779 ft, laminar	2.3	-3.2	0.3
2.8	22,000 ft/s, 247,779 ft, turbulent	-2.0	-19.4	-13.0

Table 6.6 - Other Results

No.	Scenario	Percent Error		
		Max.	Min.	Ave.
Fig. F.1: Midrange Points				
1.1	13,000 ft/s, 165,025 ft, 35°, laminar	11.2	-5.8	3.9
1.2	13,000 ft/s, 165,025 ft, 35°, turbulent	3.5	-10.8	-1.6
1.3	19,000 ft/s, 195,850 ft, 35°, laminar	9.8	-9.0	2.5
1.4	19,000 ft/s, 195,850 ft, 35°, turbulent	16.4	-4.7	7.0
Fig. F.2: Transition Scenarios				
2.1	10,000 ft/s, 156,254 ft, 25°, 4.0 ft transition point	6.2	-9.1	-2.5
2.2	16,000 ft/s, 190,000 ft, 25°, 4.0 ft transition point	0.0	0.0	0.0
2.3	22,000 ft/s, 225,000 ft, 25°, 4.0 ft transition point	10.0	-0.6	3.9
Fig. F.3: Random Scenarios				
3.1	12,000 ft/s, 151,072 ft, 20°, 3.0 ft transition point	5.4	-11.4	-1.1

Figure 6.6 Continued

No.	Scenario	Percent Error		
		Max.	Min.	Ave.
Fig. F.3: Continued				
3.2	21,000 ft/s, 196,415 ft, 30°, 8.0 ft transition point	21.3	-8.3	6.3
Fig. F.4: Out-of-Range Scenarios				
4.1	6,000 ft/s, 130,008 ft, 25°, laminar	11.5	-7.5	4.8
4.2	6,000 ft/s, 130,008 ft, 25°, turbulent	9.1	-28.7	-21.7
4.3	8,000 ft/s, 144,093 ft, 25°, laminar	11.7	-5.8	5.1
4.4	8,000 ft/s, 144,093 ft, 25°, turbulent	8.4	-19.4	-12.2
4.5	24,000 ft/s, 243,705 ft, 25°, laminar	9.6	0.1	5.0
4.6	24,000 ft/s, 243,705 ft, 25°, turbulent	0.1	-19.5	-9.9

6.2.2 Observations and Discussion

The following trends were observed when analyzing the results:

- 1) Turbulent results were generally less accurate than laminar flow results.
- 2) Lower cone-half angles had poorer results than high angles.
- 3) Adding additional angles and altitudes to the database did improve accuracy when interpolating but did not improve the results at known data points.
- 4) Adding solutions 10% higher and 10% lower than the baseline altitude to the database greatly improved results when off the trajectory.
- 5) Adding turbulent solutions along the baseline trajectory to the database did not improve velocity correlations.
- 6) Adding more data points along the baseline trajectory to improve the velocity correlation did not dramatically improve the overall results.

Based on the complexity of the extrapolation factors, it is reasonable to observe that turbulent results are less accurate than laminar results. However, if better correlations

can be developed, both laminar and turbulent flow results can be improved. In some cases a laminar extrapolation factor of unity would give better results than the extrapolation factor used (Eq. 5.28). Therefore, it is possible, with more analysis, to develop various correlations factors for different freestream velocity ranges and consequently improve results.

It was surprising to observe that lower cone-half angles had much poorer results than higher angles. A 25° cone-half angle was selected as the primary angle when computing solutions to populate the database, because it is approximately midway between the desired range of 10° and 45° cone-half angles. However, results at angles less than 20° were considerably poorer than results above 30° so more solutions were needed at lower angles. Consequently, 15° cone-half angle solutions were added to the database along with the lower and upper limits of 10° and 45° cone-half angle solutions. However, as referred to in trend 3 above, the 15° solutions did improve accuracy of interpolating between 10° and 25° but did not improve the overall results at 10° .

Since, 10° solutions were already computed in the database, adding 15° solutions to the database did not improve the extrapolated results at 10° . This is because the 10° solutions are treated as a known discreet data point so interpolation will not improve upon these values. To improve results at these angles, one would have to consider implementing different extrapolation factors or modifying the fundamental procedure.

At first, the database only had solutions along the baseline trajectory so the extrapolated results at the lower and upper limits of the freestream velocity range were generally poor when considering points above and below the trajectory. Velocity solutions were added at altitudes above and below the trajectory at these limits. Though velocity correlations were improved, improvements of overall results were minimal. Once heating solutions were added at 16,000 ft/s, the extrapolated results dramatically improved, which showed that starting with better heating solutions at Point 1 has the largest effect on the overall accuracy.

The data points at 10,000 and 22,000 ft/s were only used to determine an appropriate velocity correlation. Since the velocity at the edge of the boundary layer is the inviscid

solution, it was not necessary to calculate these values with both laminar and turbulent flow. Also, adding inviscid velocity solutions at more points along the baseline trajectory did not dramatically improve the overall results. Thus, only two points were chosen at 10,000 ft/s and 22,000 ft/s to be used with the data at 16,000 ft/s to develop cubic spline velocity correction factors.

As shown in Tables 6.3, 6.4, 6.5 and 6.6, various scenarios had percent error accuracies above the user requirement of +/-15%. However, other scenarios were well within this requirement so the freestream velocity range of xTRAP can be expanded in some instances. Therefore, based on analysis, the following table has been developed to show the acceptable operating ranges of when xTRAP functions within the desired accuracy.

Table 6.7 - xTRAP Operating Ranges

Fully Laminar or Fully Turbulent	Cone-Half Angles	Max. % Error	Freestream Velocity Range
Fully Laminar	25°-45°	10%	13,000 – 22,000 ft/s
		15%	6,000 – 24,000 ft/s
		20%	6,000 – 24,000 ft/s
Fully Turbulent	25°-45°	10%	12,000 – 18,000 ft/s
		15%	10,000 – 20,000 ft/s
		20%	9,000 – 20,000 ft/s
Fully Laminar	10°-24.9°	10%	14,000 – 18,000 ft/s
		15%	13,000 – 19,000 ft/s
		20%	11,000 – 20,000 ft/s
Fully Turbulent	10°-24.9°	10%	15,000 – 17,000 ft/s
		15%	14,000 – 18,000 ft/s
		20%	13,000 – 19,000 ft/s

These limits have been incorporated into the setup of xTRAP so the user knows what range is acceptable for a given accuracy.

As shown in Table 6.7 for cone-half angles between 25°-45°, xTRAP meets or exceeds user requirements of +/-15% over a range of 10,000 to 22,000 ft/s except for at the top of the range for turbulent flow. At these angles, turbulent results between 20,000 and 22,000 ft/s are under 22% but not under 15% error. Since, laminar results are acceptable during the full range of 10,000 to 22,000 ft/s, this error can most likely be attributed to inaccuracies in the turbulent extrapolation factors.

Cone-half angles below 25° generally had poor results. The acceptable operating range for turbulent results is limited from 14,000 to 18,000 ft/s for a maximum 15% error. If 20% error is tolerable the acceptable operating range expands to 13,000 to 19,000 ft/s, which is still short of the full desired range of 10,000 to 22,000 ft/s.

Suggestions to improve results are discussed in Section 7.2.

Chapter 7

Conclusions and Recommendations

A tool, titled xTRAP, has been developed to rapidly predict convective heating rates along a body using interpolation and extrapolation. xTRAP has proven to be successful over various ranges so the following conclusions and recommendations have been written to summarize the success of xTRAP and make suggestions to improve its functionality.

7.1 Conclusions

From a database of 26 previously calculated solutions, xTRAP is able to predict reasonably accurate laminar and turbulent convective heating rates within seconds at any point throughout the defined trajectory space. The 26 database solutions can be calculated, for a given geometry, within two days using boundary layer codes currently available. Therefore, xTRAP greatly reduces computational time and has proven to be a beneficial tool during the preliminary design of hypersonic vehicles.

7.2 Recommendations

The following recommendations are listed to improve the accuracy and expand the operation of xTRAP:

- 1) Develop more accurate laminar and turbulent extrapolation factors.
- 2) Develop a correction factor to correlate pressures at the edge of the boundary layer.

- 3) Incorporate heating results at other points along the trajectory.
- 4) Validate xTRAPs accuracy over other three-dimensional configurations.
- 5) Validate xTRAPs accuracy using other source data.
- 6) Validate the accuracy of the other resultant parameters.
- 7) Study the effects of adding radiative heating calculations.
- 8) Incorporate generalized heating equations for various geometries.

The analysis showed that, at times, the extrapolation factors chosen led to inaccuracies. Therefore, with more analysis, additional extrapolation factors could be incorporated for different freestream ranges to improve the results of xTRAP.

A correction factor was developed to correlate velocity at the edge of the boundary layer, but a correction factor was not used when extrapolating pressures at the edge of the boundary layer (Eq. 5.12). It was observed that the edge pressures were not always accurate compared to the SABLE actual data so adding a correction factor to edge pressures could improve xTRAP's results.

Points along the trajectory were used to develop the velocity correction factors but the known surface heating rates at those points were not used. Incorporating these known values would change the extrapolation procedure but, in some circumstances, they could improve results without adding any additional points to the database.

xTRAP has only been tested using a spherical blunted-nose axisymmetric cone, so testing xTRAP with other three-dimensional configurations is recommended. Also, xTRAP only used SABLE¹⁴ to generate the solutions in the database, so testing xTRAP with other source data is recommended.

As mentioned in Section 5.2.6, multiple parameters are calculated during the analysis to determine the surface heating rates. These parameters, such as wall temperature, could also be useful during preliminary design of hypersonic vehicles so it is recommended to validate their accuracy compared to the source data.

The focus of xTRAP was to predict convective heating rates at the surface of a body, but adding radiative heating predictions would make xTRAP a more complete preliminary design tool. The procedure used to extrapolate the surface heating rates can be applied to either convective or radiative heating at the surface, but the results have not been validated for radiative heating.

As shown in Section 3.3.2, generalized heating equations have only been developed for a few basic shapes but if more generalized heating equations could be developed and incorporated into xTRAP then the efficiency could greatly improve.

References

- [1] National Aeronautics and Space Administration, *Report Volume 1 - Columbia Accident Investigation Board*. August 2003. Web. 17 Nov. 2010.
- [2] Bertin, John J., *Hypersonic Aerodynamics*. AIAA Education Series, Washington, DC, 1994.
- [3] Hamilton, H. H, Weilmuenster, K. J., DeJarnette, F. R., "Improved Approximate Method for Computing Convective Heating on Hypersonic Vehicles Using Unstructured Grids." AIAA-2006-3394, June 2006.
- [4] Hamilton, H. H, Weilmuenster, K. J., DeJarnette, F. R., "Approximate Method for Computing Laminar and Turbulent Convective Heating on Hypersonic Vehicles Using Unstructured Grids." AIAA-2009-4310, June 2009.
- [5] Palmer, Grant, "Adding CFD-Based Correction Factors to Engineering Datasets Using the ADSI Code." AIAA-2006-3770, June 2006.
- [6] Palmer, Grant, "Construction of CFD Solutions Using Interpolation Rather than Computation with the ADSI Code." AIAA-2009-141, January 2009.
- [7] Anderson, John D., Jr. *Introduction to Flight*, 6th Ed. McGraw-Hill, New York, 2005.
- [8] Lees, Lester, "Laminar Heat Transfer Over Blunt-Nose Bodies at Hypersonic Flight Speeds," AIAA Journal Special Supplement: Centennial of Powered Flight (Jet Propulsion), Vol. 26, No. 4. 1956, pp. 357.
- [9] Anderson, John D., Jr. *Hypersonic and High-Temperature Gas Dynamics*, 2nd Ed. American Institute of Aeronautics and Astronautics, Inc., Reston, Va, 2006.
- [10] Sforza, P. M., *EAS4710 Aerospace Design II, Chapter 6 Course Notes*. January 2009. Web. 30 Sep. 2010.
- [11] Tauber, M. E. and Sutton, K., "Stagnation Point Radiative Heating Relations for Earth and Mars Entries." *Journal of Spacecraft and Rockets*, Vol. 28, No. 1. 1991. pp. 1.
- [12] Anderson, John D., Jr. *Computational Fluid Dynamics: The Basics with Applications*. McGraw-Hill, New York, 1995, pp. 4.
- [13] Cheatwood, F. M. and Gnoffo, P. A., "User's Manual for the Langley Aerothermodynamic Upwind Algorithm (LAURA)," NASA TM-4674, April 1996.

- [14] Hamilton, H. H., Millman, D. R., Greendyke, R. B., "Finite-Difference Solution for Laminar and Turbulent Boundary Layer Flow Over Axisymmetric Bodies With Ideal Gas, CF_4 , or Equilibrium Air Chemistry" NASA Technical Paper 3271, 1992.
- [15] Hamilton, H. H., Spall, J. R., "Time-Dependent Solution for Axisymmetric Flow Over a Blunt Body With Ideal Gas, CF_4 , or Equilibrium Air Chemistry" NASA Technical Paper 3271, July 1986.
- [16] Hamilton, H. H., DeJarnette, F. R., and Weilmuenster, K. J., "Application of Axisymmetric Analog for Calculating Heating in Three-Dimensional Flows," *Journal of Spacecraft and Rockets*, Vol. 24, No. 4, 1987, pp. 296-302.
- [17] Hamilton, H. H., Greene, F. A., and DeJarnette, F. R., "Approximate Method for Calculating Heating Rates on Three-Dimensional Vehicles," *Journal of Spacecraft and Rockets*, Vol. 31, No. 3, 1994, pp. 345-354.
- [18] Cooke, J. C., "An Axially Symmetric Analogue for General Three-Dimensional Boundary Layers," Reports and Memoranda No. 3200, British Aeronautical Research Council, 1961.
- [19] Inger, G. R. and Gnoffo, P. R., "Hypersonic Entry Heating with Discontinuous Surface Catalycity: A Combined Analytical/CFD Approach," AIAA 96-2150, June 1996.
- [20] Fay, J.A. and Riddell, F.R.: "Theory of Stagnation Point Heat Transfer in Dissociated Air", *Journal of the Aeronautical Sciences*, Vol. 25, No. 2, February, 1958, pp. 73-85.
- [21] Van Driest, E. R., "The Problem of Aerodynamic Heating," *Aeronautical Engineering Review*, Oct. 1956, pp. 26-41.
- [22] Tauber, M. E. and Meneses, G. P., "Aerothermodynamics of Transatmospheric Vehicles," AIAA Paper 86-1257, June 1986.
- [23] Sutton, K. and Graves, R.A.: "A General Stagnation-Point Convective-Heating Equation for Arbitrary gas Mixtures", NASA TR R-376, 1971.
- [24] Hamilton, H. H, personal communication, Raleigh, NC, August 2010.
- [25] Merski, N. R., "Reduction and Analysis of Phosphor Thermography Data With IHEAT Software Package," AIAA-1998-0712, January 1998.
- [26] Kreyszig, Erwin, *Advanced Engineering Mathematics*, Eighth Edition. John Wiley & Sons, Inc, New York, 1999, pp. 848-862.
- [27] DeJarnette, F. R., *MAE451 Boundary Layer Theory, Course Notes*. Raleigh, NC, August 2010.

[28] National Aeronautics and Space Administration, *U.S. Standard Atmosphere, 1972*, NASA-TM-X-74335, Washington, DC, October 1976.

Appendices

Appendix A - Cubic Spline Algorithm

Option Base 1

```
'  
' Appendix A - Cubic Spline Algorithm  
'  
' Kurt Whittington  
' Rev. 1. (based on SRS1 Software)  
' 3/21/2011  
'  
' icolumn = range of inputs  
' ocolumn = range of outputs  
' icount = number of inputs  
' ocount = number of outputs  
' xin = x values  
' yin = y values  
  
Function cubic_spline(icolumn As Range, ocolumn As Range, X As Range)  
  
' Description:  
' Given a x-column and a y-column in increasing order, this function  
' interpolates a y-output from a new given x-input value.  
  
Dim icount As Integer  
Dim ocount As Integer  
Dim c As Integer  
Dim n As Integer 'n = icount  
Dim I, k As Integer 'loop counting integers  
Dim p, qn, sig, un As Single  
Dim klo, khi As Integer  
Dim h, b, a As Single  
  
' Counts number of input and output data points  
icount = icolumn.Rows.Count  
ocount = ocolumn.Rows.Count  
  
' Verify input and output number of points are equal  
If icount <> ocount Then  
    cubic_spline = "Column numbers don't match"  
    GoTo out  
End If  
ReDim xin(icount) As Single  
ReDim yin(icount) As Single  
For c = 1 To icount  
    xin(c) = icolumn(c)  
    yin(c) = ocolumn(c)  
Next c  
  
' Populate values  
ReDim u(icount - 1) As Single
```

```

ReDim yt(icount) As Single '2nd deriv values
n = icount
yt(1) = 0
u(1) = 0

For I = 2 To n - 1
    sig = (xin(I) - xin(I-1)) / (xin(I+1) - xin(I-1))
    p = sig * yt(I - 1) + 2
    yt(I) = (sig - 1) / p
    u(I) = (yin(I+1) - yin(I)) / (xin(I+1) - xin(I)) - (yin(I) - yin(I-1)) / (xin(I) - xin(I-1))
    u(I) = (6 * u(I) / (xin(I+1) - xin(I-1)) - sig * u(I-1)) / p
Next I
qn = 0
un = 0
yt(n) = (un - qn * u(n-1)) / (qn * yt(n-1) + 1)
For k = n - 1 To 1 Step -1
    yt(k) = yt(k) * yt(k+1) + u(k)
Next k

' Evaluate spline at one point
klo = 1
khi = n
Do
    k = khi - klo
    If xin(k) > X Then
        khi = k
    Else
        klo = k
    End If
    k = khi - klo
Loop While k > 1
h = xin(khi) - xin(klo)
a = (xin(khi) - X) / h
b = (X - xin(klo)) / h
Y = a * yin(klo) + b * yin(khi) + ((a^3 - a) * yt(klo) + (b^3 - b) * yt(khi)) * (h^2) / 6

cubic_spline = Y
out:

End Function

```

Appendix B - xTRAPs Main Screen (Screenshot)

eXtrapolate Thermal Reentry Atmosphere Parameters (xTRAP)

This preliminary design tool has been developed by Kurt Whittington, Aerospace Engineering graduate student at NC State University. © 2011.

Disclaimer: The results are only as accurate as the data supplied. Therefore, the results should not be used for any final design considerations.

Input the following white boxes: (all lowercase)

Value	Comments
Initial Setup:	
Fluid Flow Profile: transition	Choose fully laminar, fully turbulent or transition.
Maximum % error: 15%	Choose either 10%, 15% or 20%
Allowable Altitude Deviation from Baseline Trajectory: 10%	Choose either 5 or 10%
Lower Angle-of-Attack Limit: 25.0 deg	Minimum value is 10 degrees
Upper Angle-of-Attack Limit: 45.0 deg	Maximum value is 45 degrees
Lower Velocity Limit of Trajectory Space: 10,000.00 ft/s	Minimum value 10,000.00 ft/s
Upper Velocity Limit of Trajectory Space: 20,000.00 ft/s	Maximum value 20,000.00 ft/s
Has the baseline trajectory data been supplied?: yes	Trajectory data is supplied in tab labeled 'Traj'
Source Data:	
Data points needed to ensure % error:	Points on Baseline Trajectory
Known Points: 15,000.00 ft/s	184,675 ft
Velocity Correlation Point 1: 10,000.00 ft/s	156,254 ft
Velocity Correlation Point 2: 20,000.00 ft/s	211,951 ft
Velocity Correlation Point 3: N/A ft/s	N/A ft
Total number of data points needed: 15	Total number of data points needed.
Has the source data been supplied?: yes	Known data is supplied in column form in the appropriate tabs.
Freestream Conditions:	
X-Velocity: 16,000.00 ft/s	Must be between velocity limits listed above.
Baseline altitude @ this velocity: 190,000 ft	Calculated based on baseline trajectory data
Minimum Altitude @ this velocity: 171,000 ft	Calculated based on allowable deviation % specified above.
Maximum Altitude @ this velocity: 209,000 ft	Calculated based on allowable deviation % specified above.
Altitude: 190,000 ft	Must be between minimum and maximum altitudes above.

Parameter to Extrapolate: qw

Surface Body Position:

Distance	Comments
1	
2	0.50 ft
3	1.00 ft
4	1.50 ft
5	2.00 ft
6	2.50 ft
7	3.00 ft
8	3.50 ft
9	4.00 ft
10	4.50 ft
Surface distance to transition	15.00 ft

Note: This assumes an axisymmetric body so only one distance is needed to define a location. Otherwise a unique identifier can be created based on x,y,z position.

Positions greater are turbulent. Suggested N/A

Calculate

Click to calculate the solution.

Results:

Fluid Profile	Surface Distance	qw
Laminar	0.00 ft	45.02E+0 BTU/(ft ² -s)
Laminar	0.50 ft	43.01E+0 BTU/(ft ² -s)
Laminar	1.00 ft	37.20E+0 BTU/(ft ² -s)
Laminar	1.50 ft	28.12E+0 BTU/(ft ² -s)
Laminar	2.00 ft	18.08E+0 BTU/(ft ² -s)
Laminar	2.50 ft	11.75E+0 BTU/(ft ² -s)
Laminar	3.00 ft	09.80E+0 BTU/(ft ² -s)
Laminar	3.50 ft	08.95E+0 BTU/(ft ² -s)
Laminar	4.00 ft	08.54E+0 BTU/(ft ² -s)
Laminar	4.50 ft	08.35E+0 BTU/(ft ² -s)

Appendix C - 25° Cone-Half Angle Plotted Results

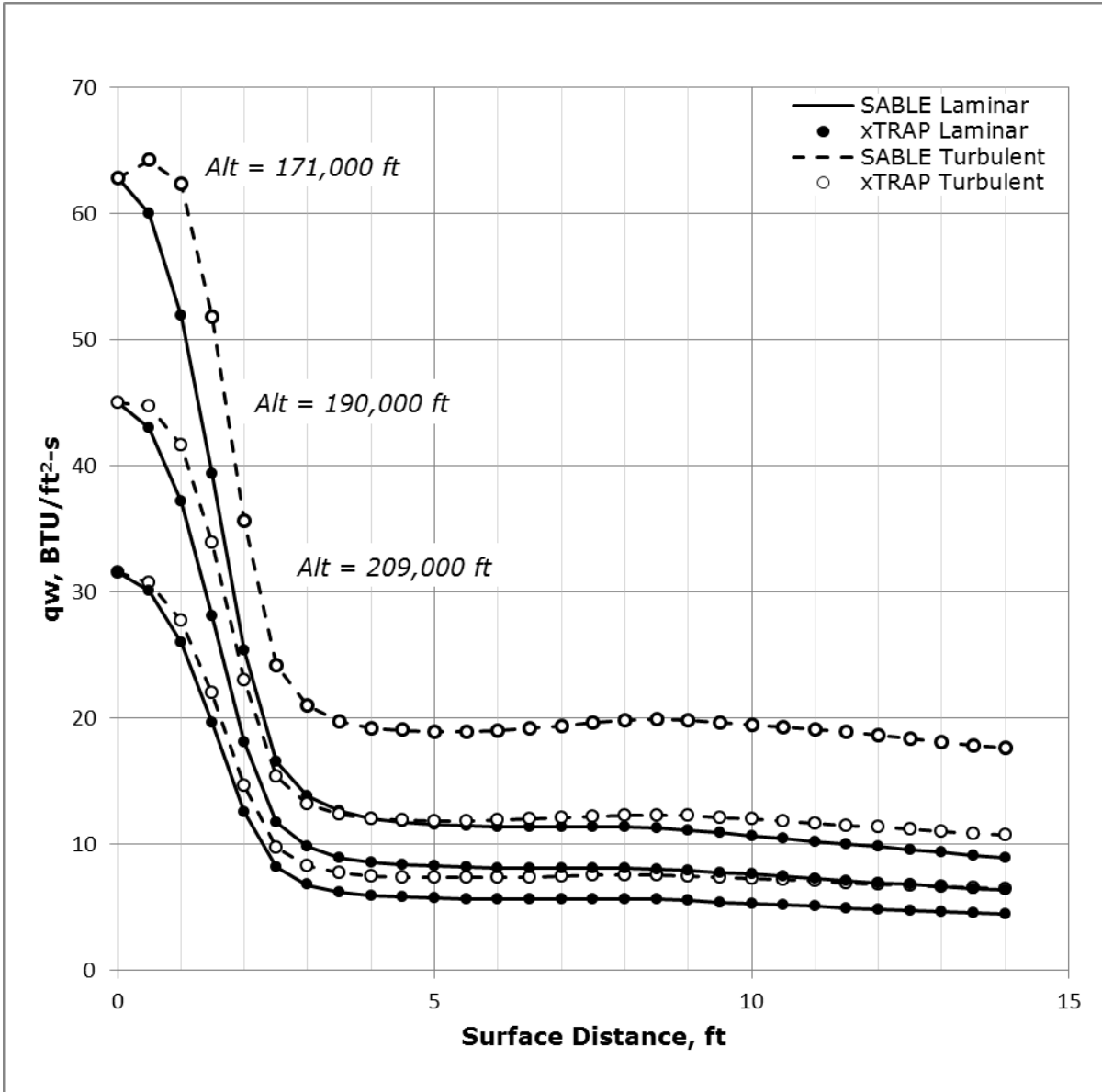


Figure C.1 - 25° Results: Known Trajectory Points at $V_\infty = 16,000$ ft/s

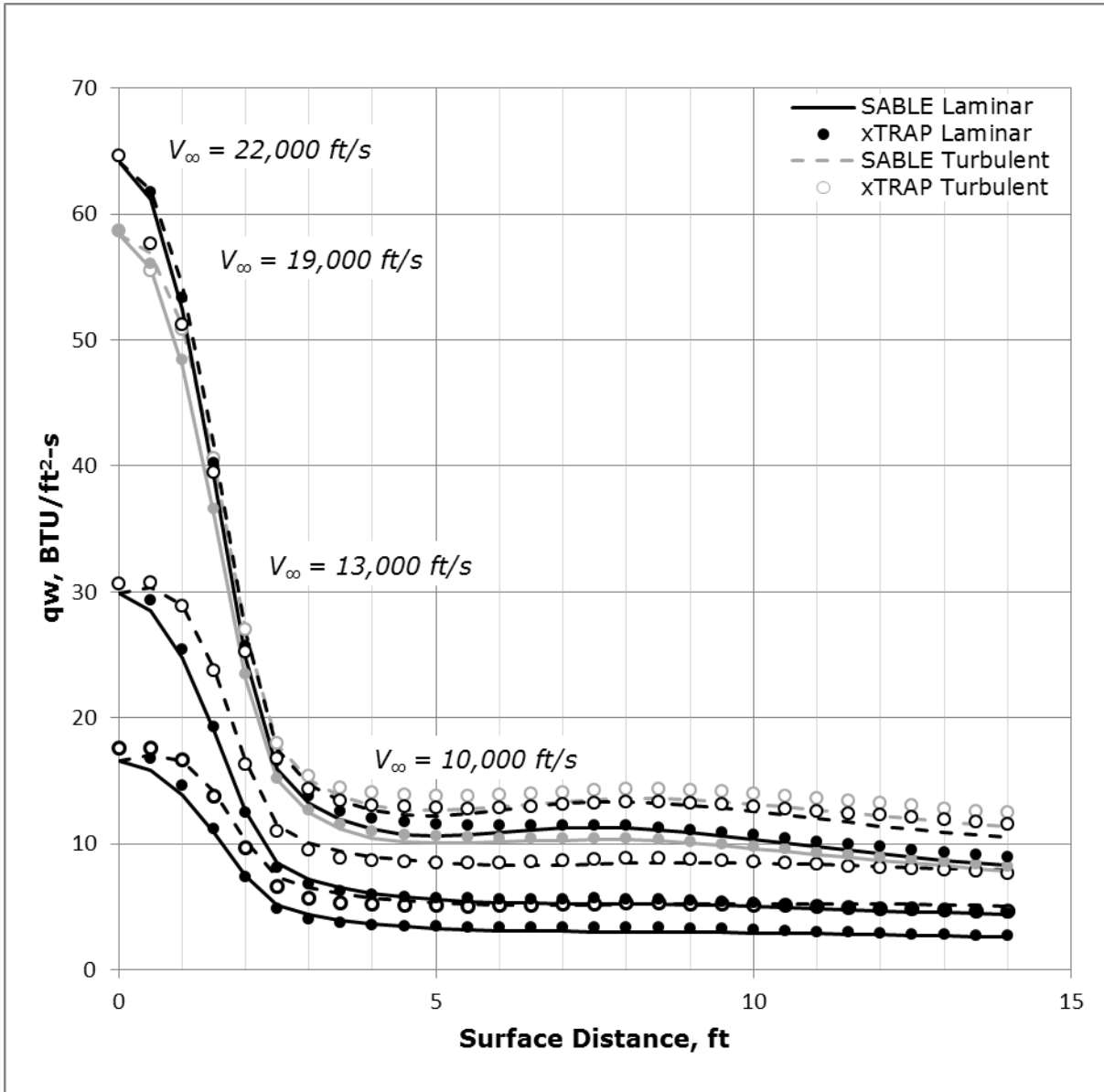


Figure C.2 - 25° Results: Baseline Trajectory Points

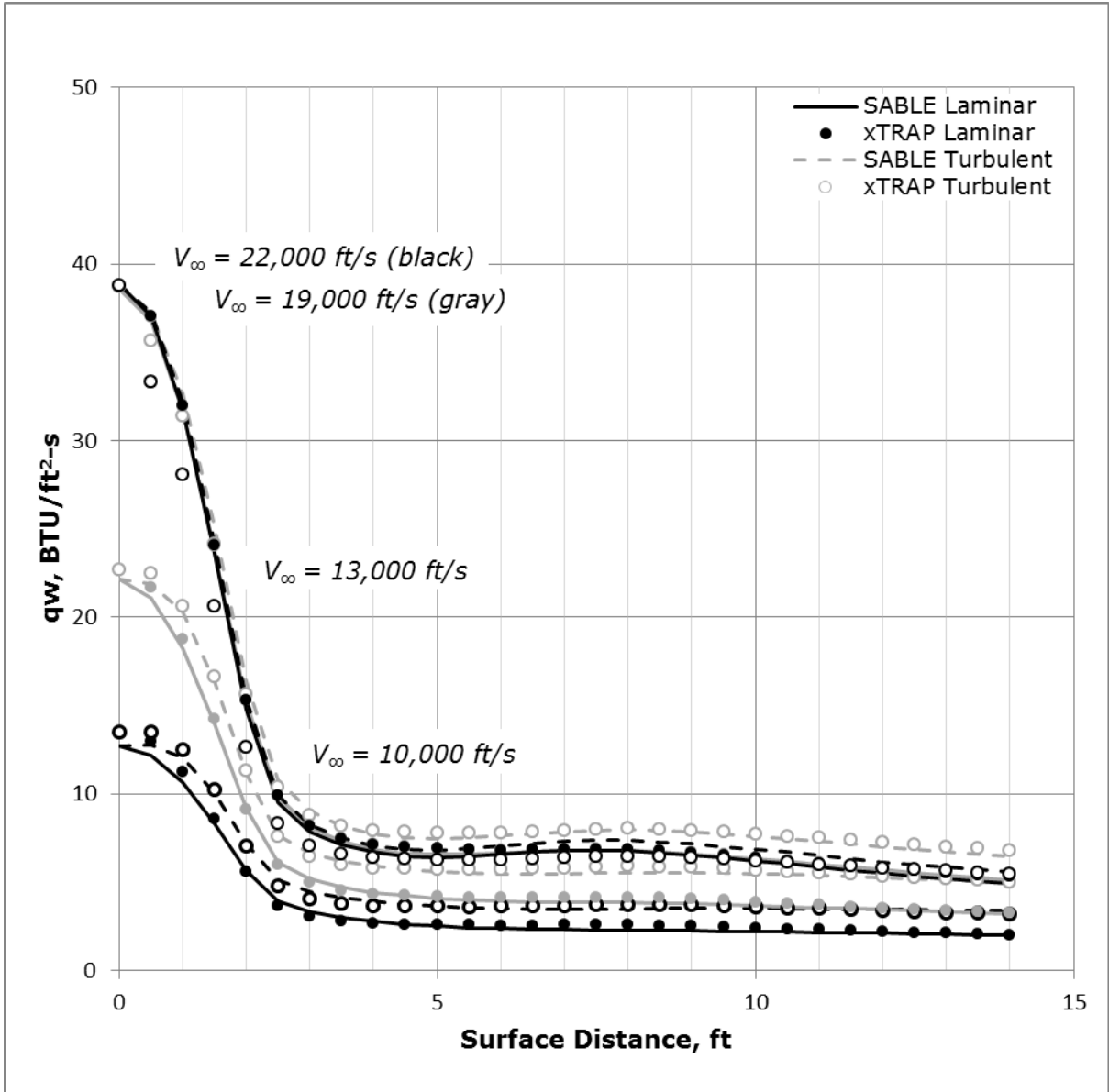


Figure C.3 - 25° Results: 10% Above Baseline Trajectory

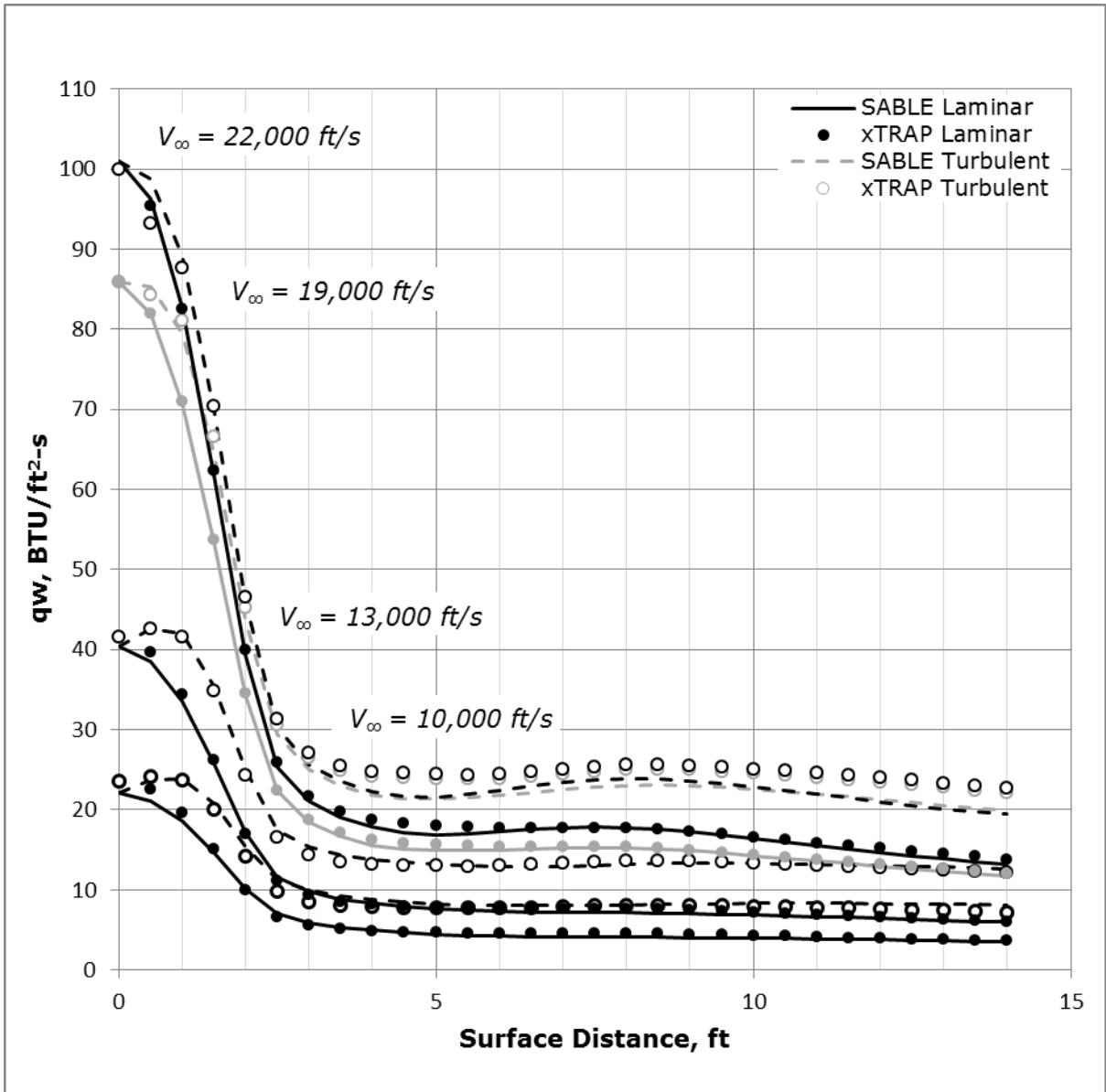


Figure C.4 - 25° Results: 10% Below Baseline Trajectory

Appendix D - 10° Cone-Half Angle Plotted Results

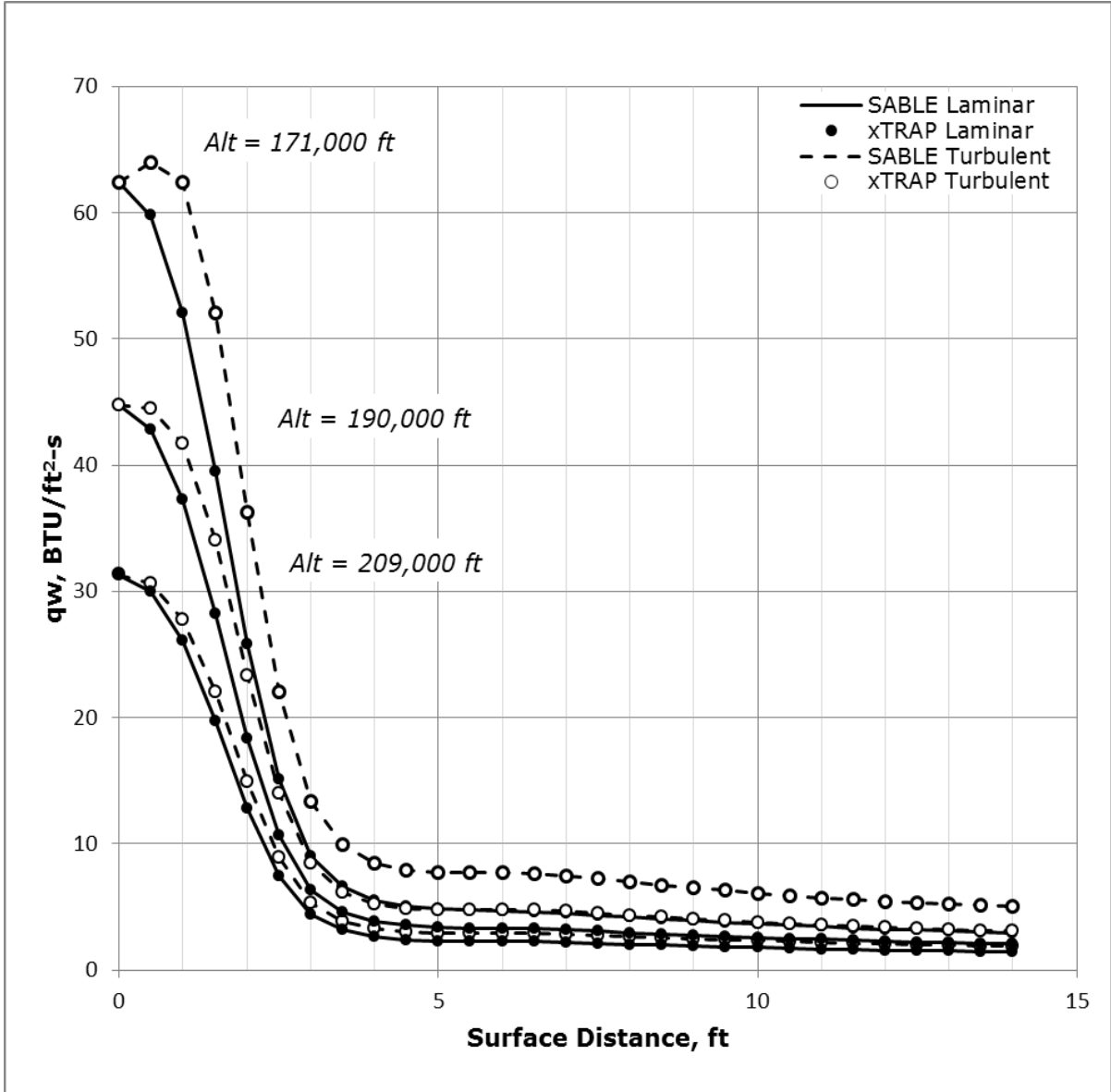


Figure D.1 - 10° Results: Known Trajectory Points at $V_\infty = 16,000$ ft/s

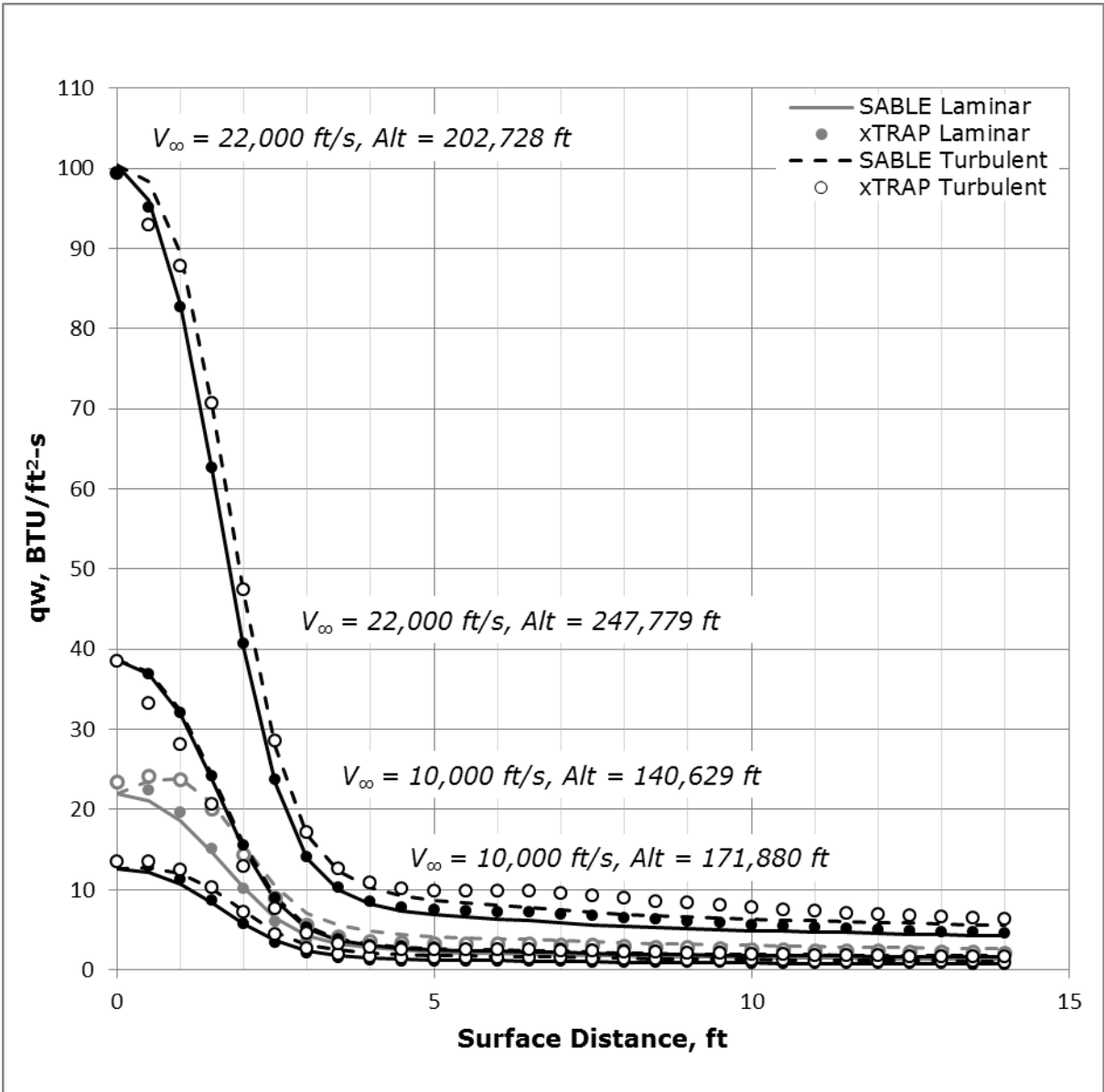


Figure D.2 - 10° Results: 10% Above and Below Baseline Trajectory

Appendix E - 45° Cone-Half Angle Plotted Results

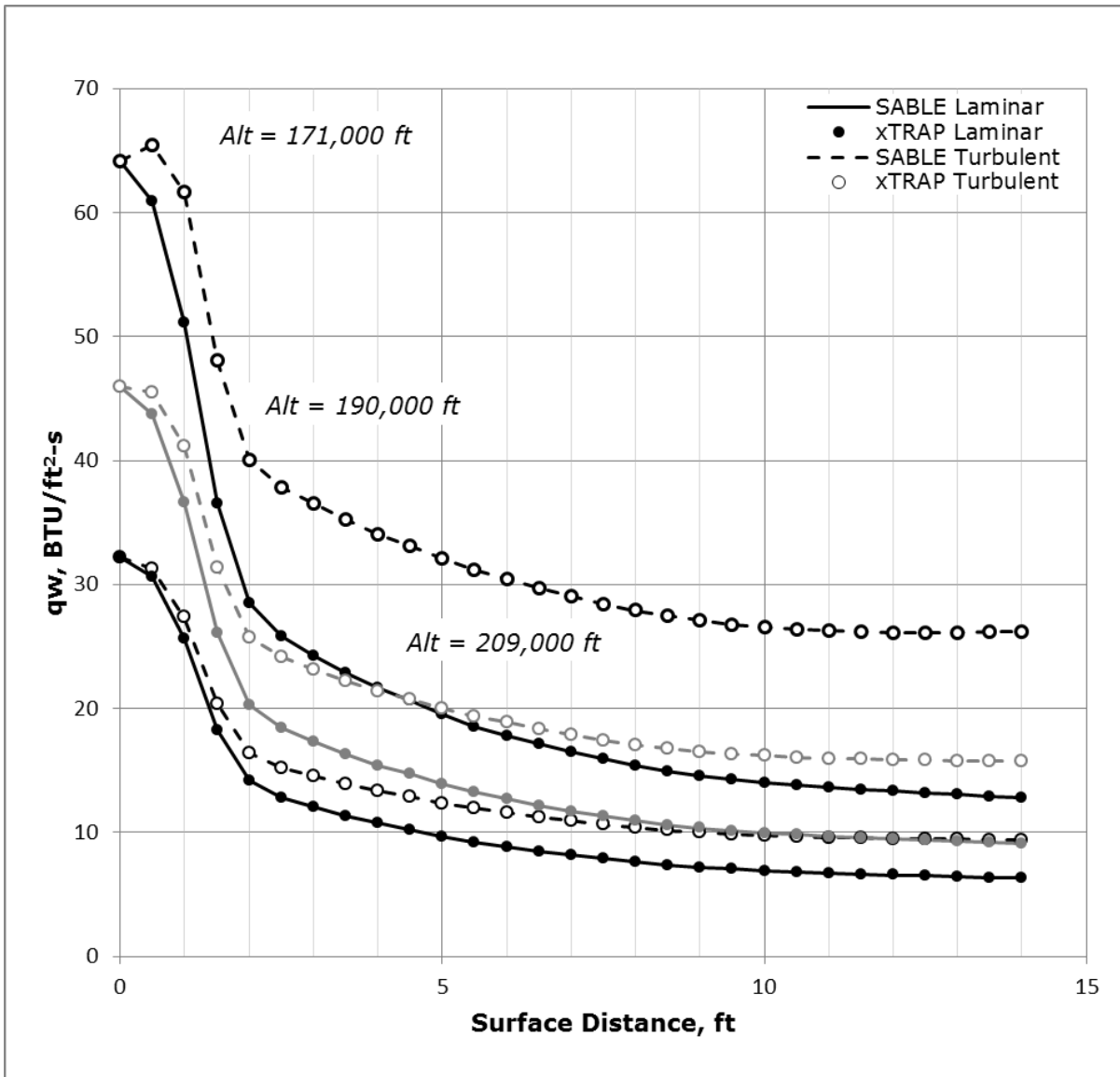


Figure E.1 - 45° Results: Known Trajectory Points at $V_\infty = 16,000$ ft/s

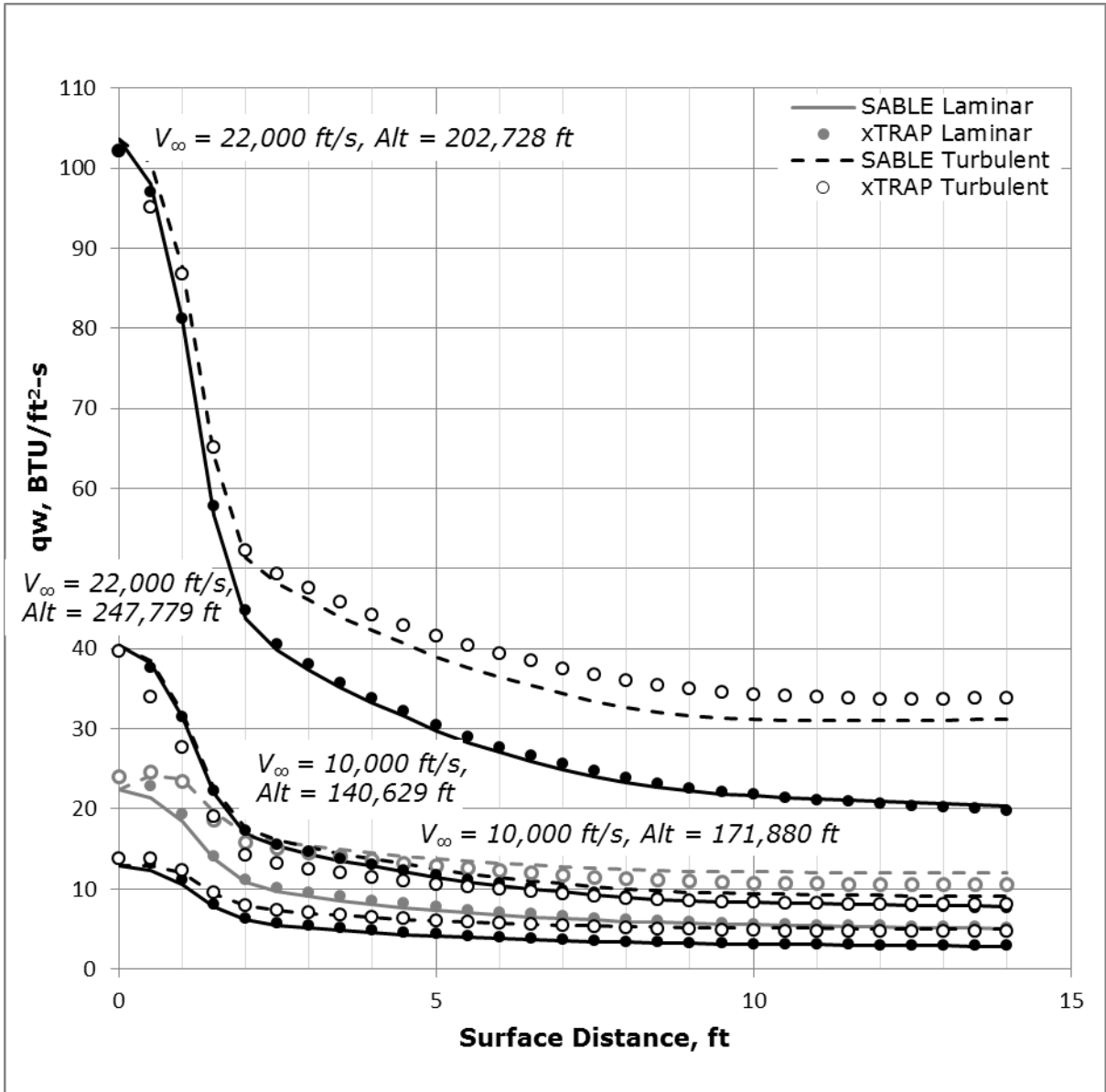


Figure E.2 - 45° Results: 10% Above and Below Baseline Trajectory

Appendix F - Other Plotted Results

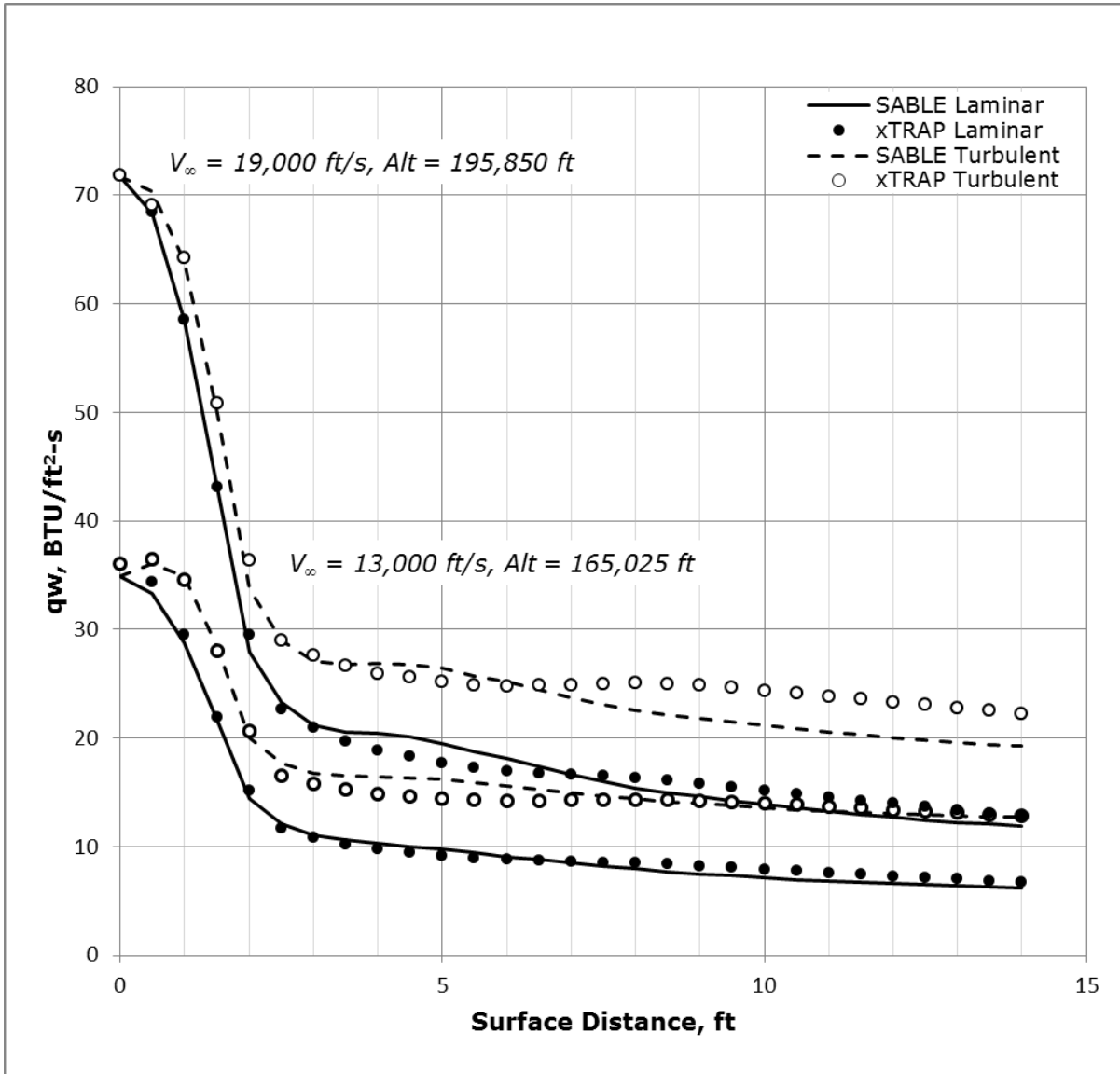


Figure F.1 - Other Results: Midrange Points, 35° Cone-Half Angle

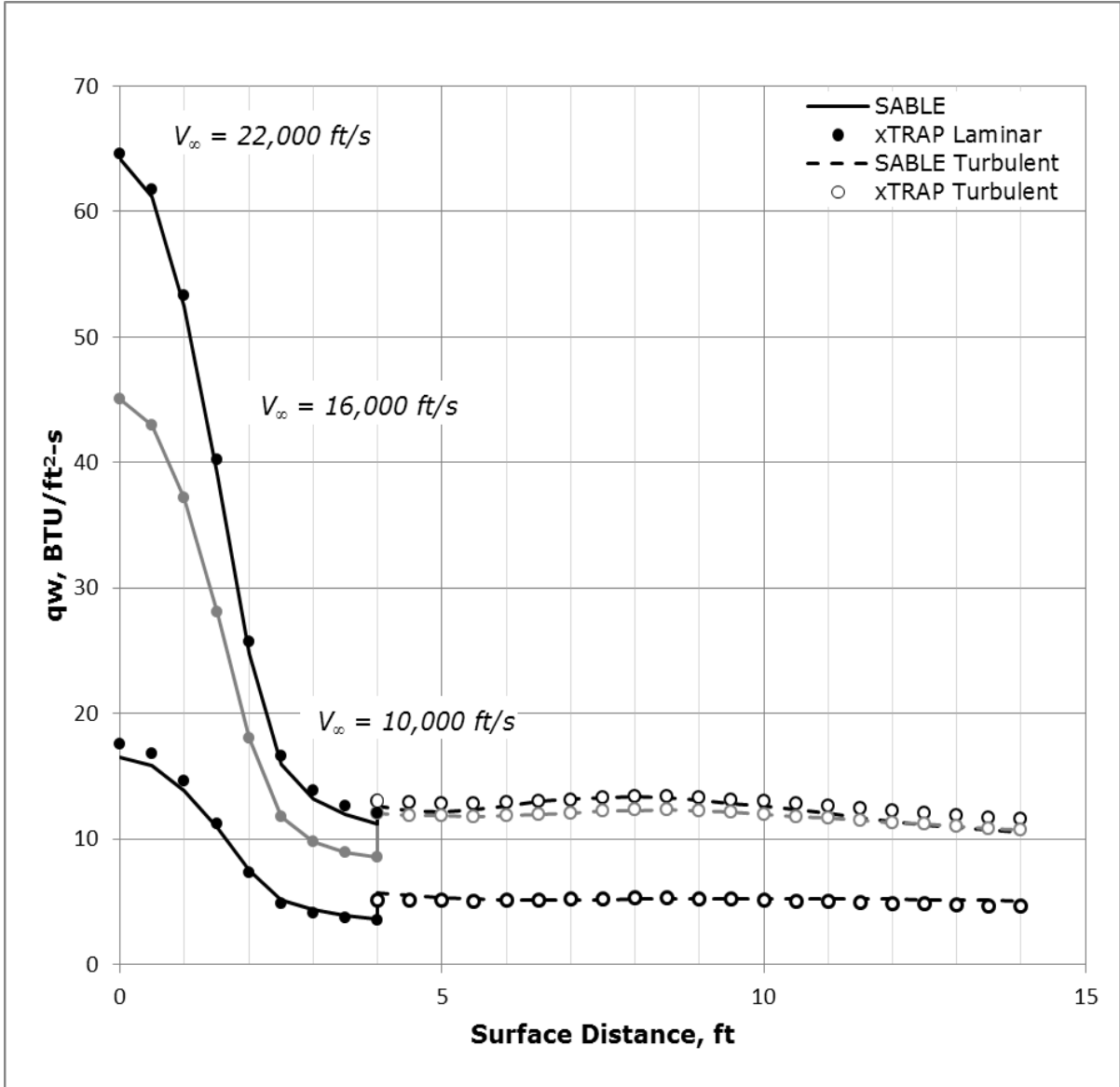


Figure F.2 - Other Results: Transition Point Examples ($x_t = 3.0$ ft)

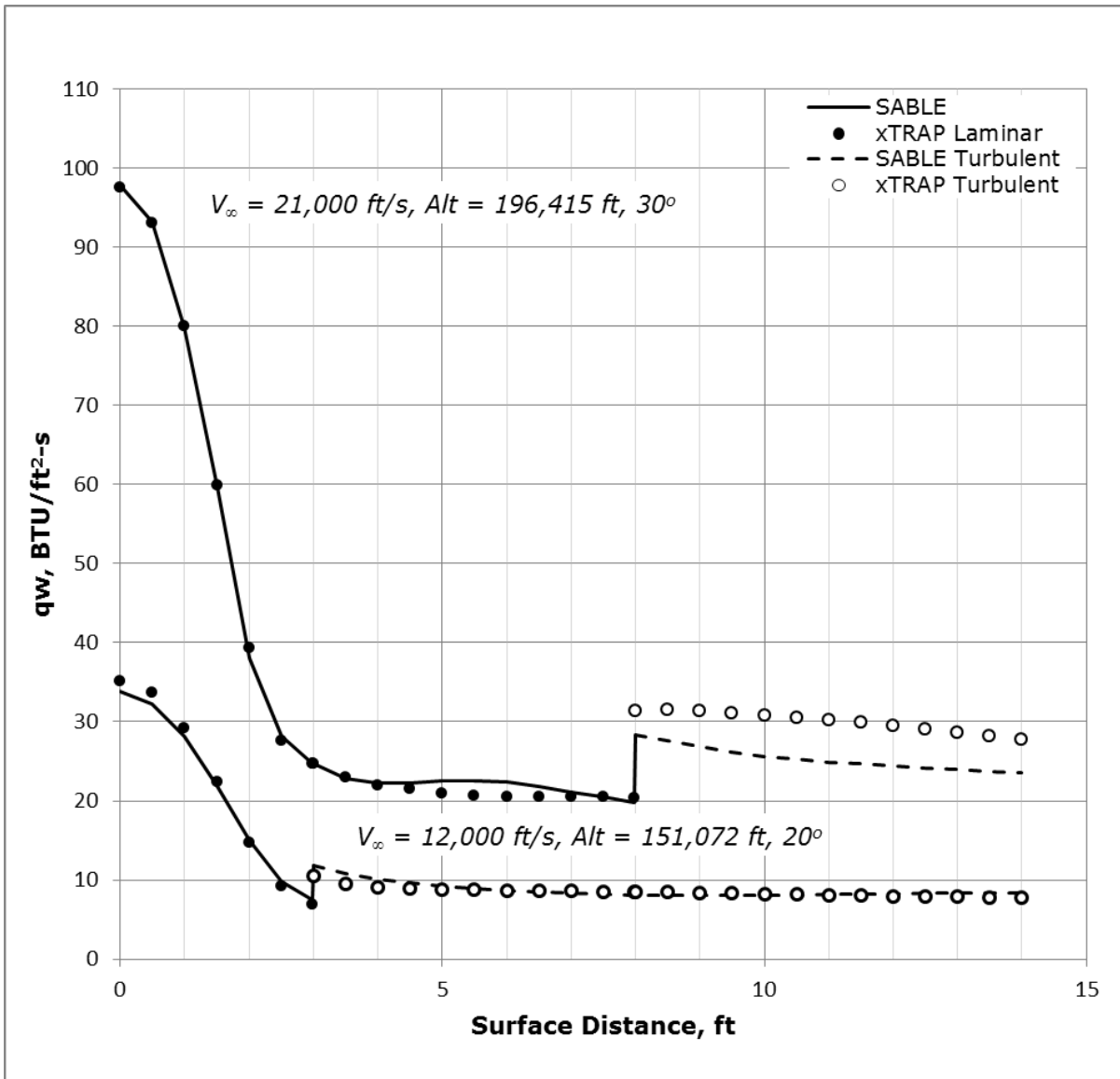


Figure F.3 - Other Results: Random Scenarios

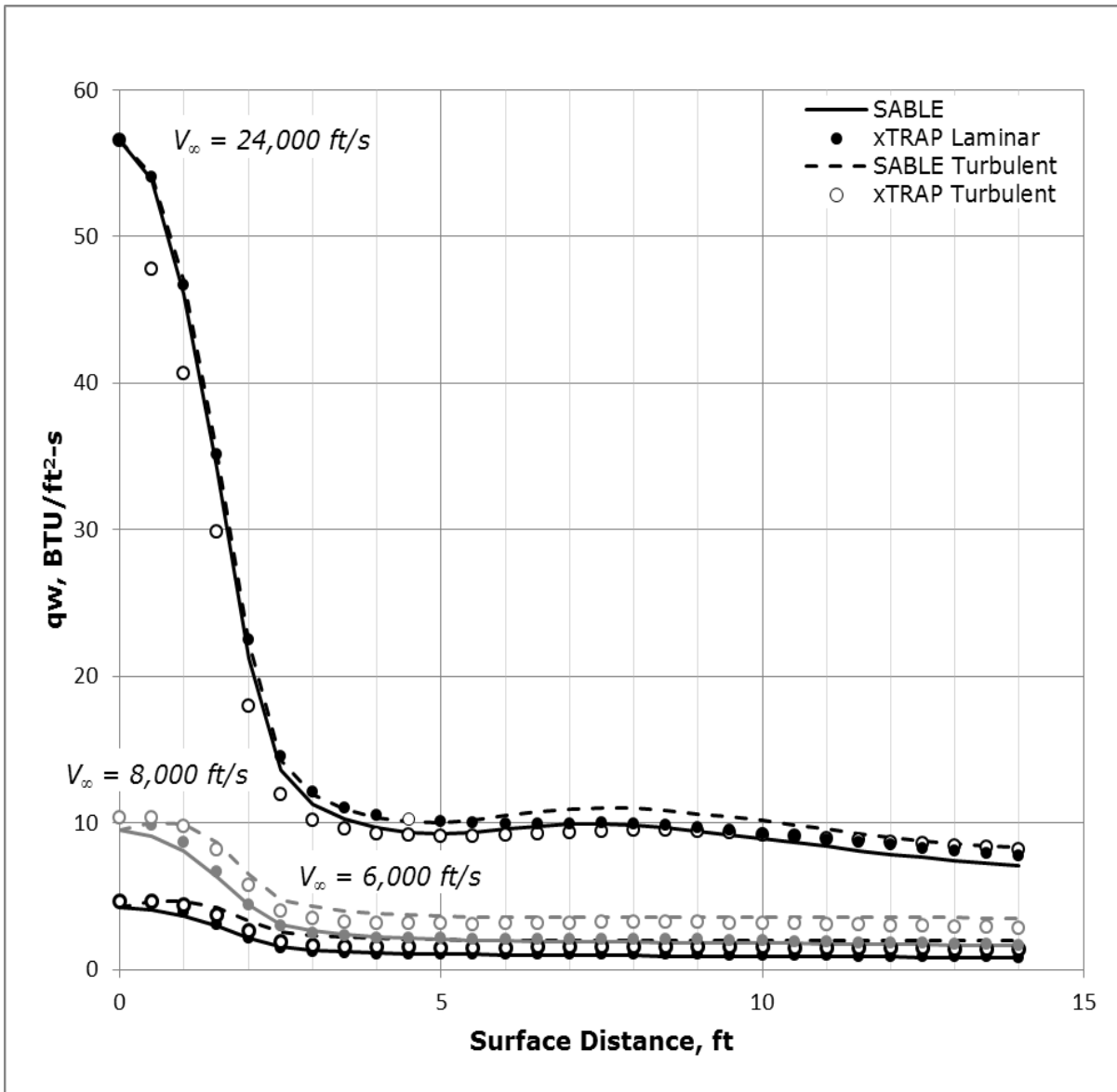


Figure F.4 - Other Results: Out-of-Range Scenarios, 25° Baseline